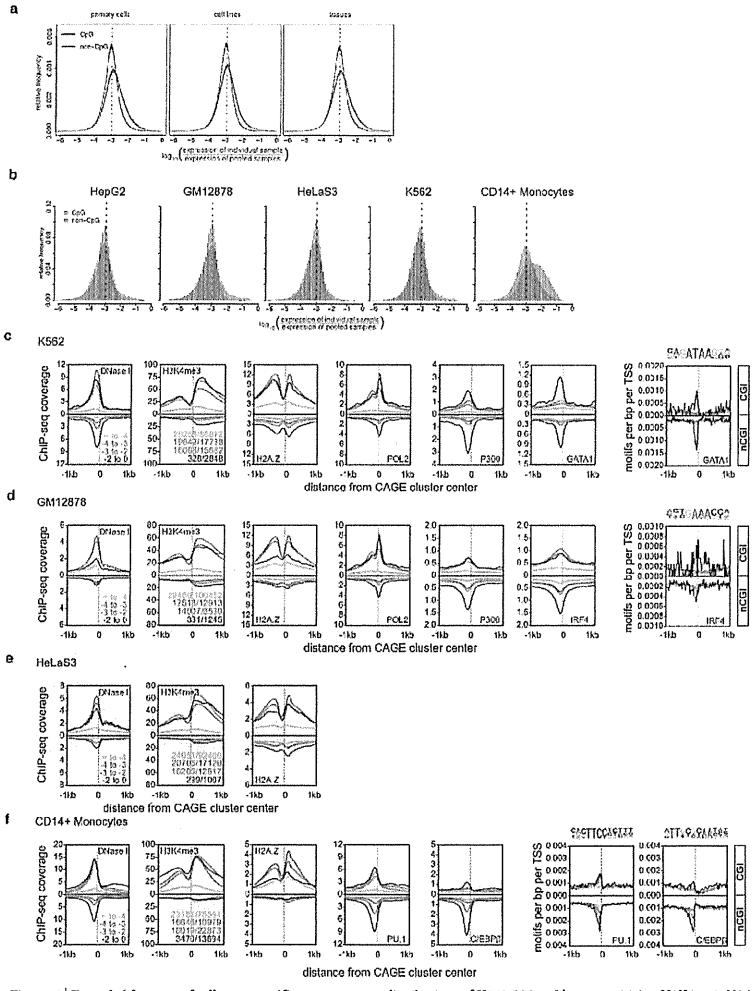

Extended Data Figure 7 | Extended features of cell-type-specific promoters. a, Distribution of global expression specificity estimated using primary cells, cell lines or tissues only. b, Distribution of expression specificity for HepG2, GM12878, HeLaS3, K562 and CD14^{+} monocytes (distribution of expression log ratios of all individual samples against the median of all samples is shown separately for CGI-associated and nonCGI-associated CAGE clusters. The dashed line corresponds to an expected log ratio if all samples contribute equally to the total expression). c, Histograms for genomic distance distributions of K562 DNase I hypersensitivity, H3K4me3, H2A.Z, POL2, P300, GATA1 ChIP-seq tag counts centred across CGI-associated and non-CGI-associated CAGE clusters (separated according to expression specificities) across a 2 kb genomic region. Expression specificity bins are colour-coded with blue representing the highest degree of specificity. d, DNase I hypersensitivity, H3K4me3, H2A.Z, POL2, P300 and IRF4 in GM12878. e, DNase I hypersensitivity, H3K4me3, H2A.Z in HeLaS3. f, DNase I hypersensitivity, H3K4me3, H2A.Z, PU.1 and CEBPB in CD14^{+} monocytes.

©2014 Macmillan Publishers Limited. All rights reserved

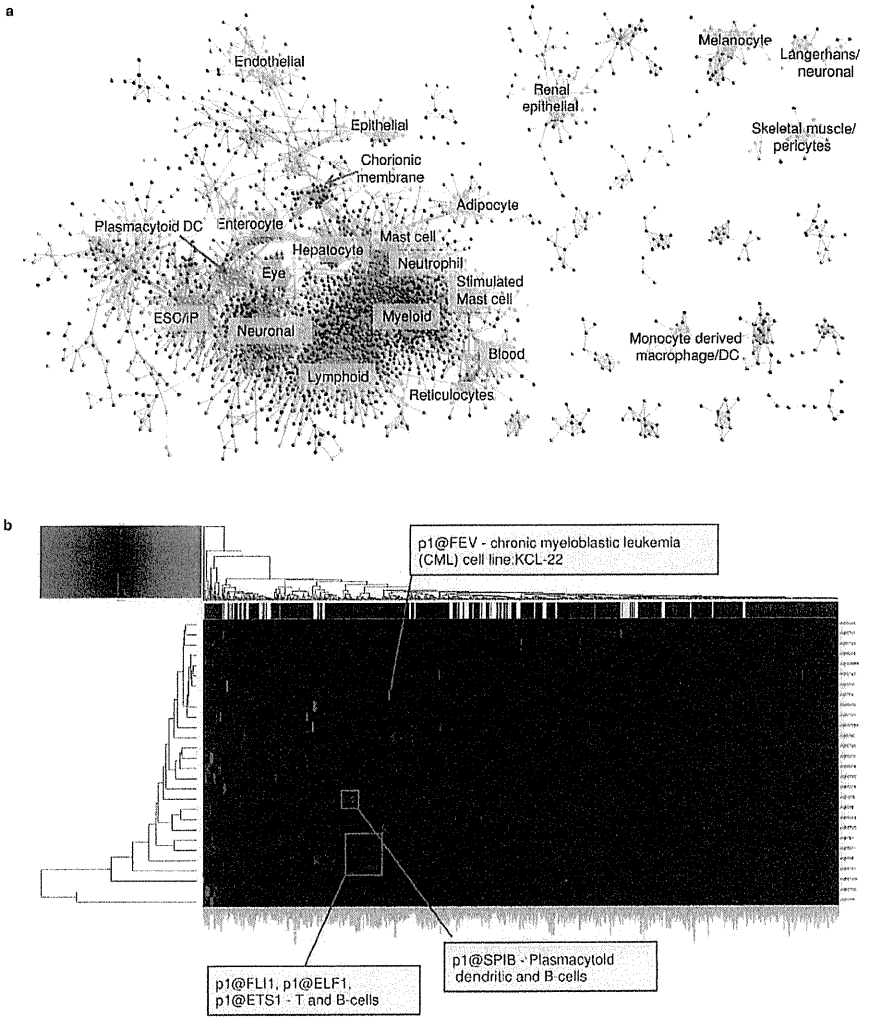

Extended Data Figure 8 | Transcription factor promoter expression profile clustering. a, Biolayout visualization of transcription factor coexpression in human primary cells (3,775 nodes, 54,892 edges $r > 0.70$, MCL2.2). b, Hierarchical coexpression clustering and heatmap of ETS family transcription factors across the entire human collection (only promoter1(p1) data shown).

©2014 Macmillan Publishers Limited. All rights reserved

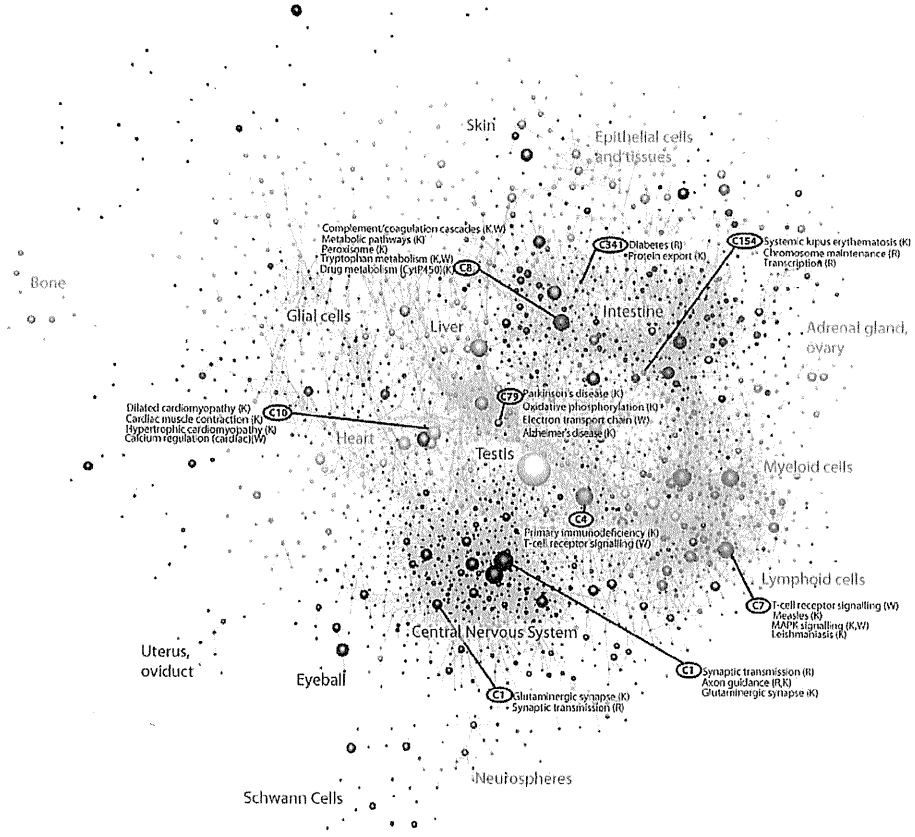

Extended Data Figure 9 | Collapsed coexpression network for mouse coexpression groups. One node is one group of promoters. Derived from expression profiles of 116,277 promoters across 402 primary cell types, tissues and cell lines ($r > 0.75$, MCLi = 2.2). For display, each group of promoters is collapsed into a sphere, the radius of which is proportional to the cube root of the number of promoters in that group. Edges indicate $r > 0.6$ between the average expression profiles of each cluster. Colours indicate loosely-associated collections of coexpression groups (MCLi = 1.2). Labels show representative descriptions of the dominant cell type in coexpression groups in each region of the network, and a selection of highly-enriched pathways (FDR $< 10^{-5}$) from KEGG (K), WikiPathways (W), Netpath (N) and Reactome (R).

©2014 Macmillan Publishers Limited. All rights reserved

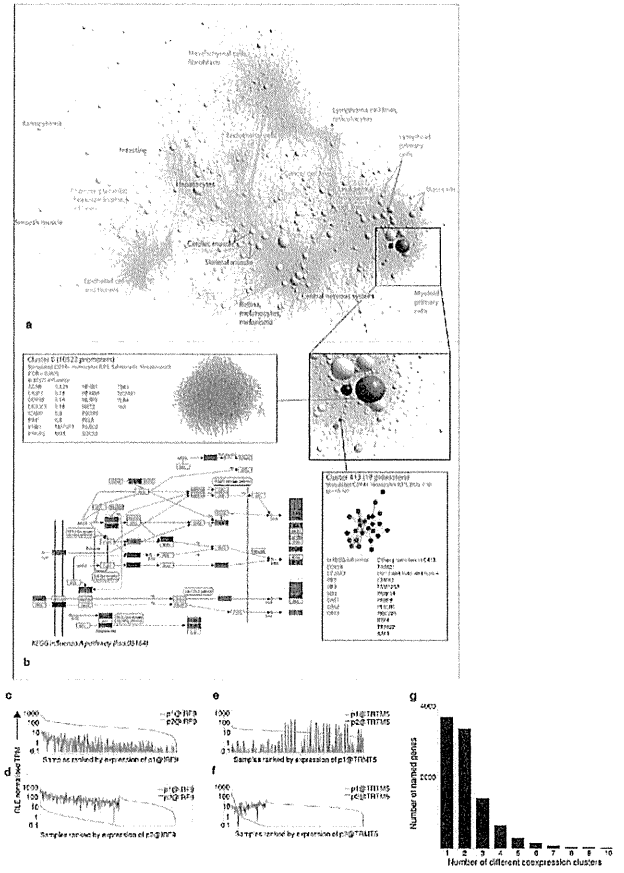

Extended Data Figure 10 | Annotated expression profiles of alternative promoters. Overlay of coexpression groups enriched for genes involved in the KEGG pathway for influenza A pathogenesis (hsa:05164; FDR < 0.1, $n > 2$). **a**, Collapsed coexpression network showing 5 groups enriched for influenza pathogenesis genes: C0 (blue), C26 (purple), C61 (yellow), C187 (green) and C413 (red). **b**, Excerpt from KEGG pathway diagram showing positions of genes in each coexpression group (background colours as in **a**). Pathway entities that map to two coexpression groups have the background colour of the smaller group, and the text/border colour of the larger group. Details and promoter-level displays (edges indicate $r > 0.75$) for two coexpression groups are displayed with transcripts mapping to KEGG pathway highlighted (inset). In this example the KEGG pathway for influenza A pathogenesis (hsa:05164) was strikingly over-represented in one small coexpression group in particular (C413, P value $< 10^{-11}$, FDR $= 4.5 \times 10^{-10}$). Of 19 promoters in coexpression group 413, eight were present in the KEGG pathway, including RIG-I (*DDX58*), the gene encoding the receptor for the mitochondrial antiviral signalling pathway[53]. Four of the remaining genes (*TRIM21*, *TRIM22*, *RTP4* and *XAF1*) were found to be key host determinants of influenza virus replication in a high-throughput short interfering RNA (siRNA) screen[54], whereas another, *PLSCR1*, is required for a normal interferon response to influenza A[55]. The top five transcription factor expression profiles most correlated with C413 were *IRF7*, *IRF9*, *STAT1*, *SP100* and *ZNFX1*, and from motif enrichment analysis, the most frequent motifs found in promoters of cluster C413 were potential IRF-binding motifs. **c**, p1@IRF9 and p2@IRF9 expression ranked by the ubiquitously expressed p1@IRF9 promoter. **d**, As in **a** but ranked by expression of p2@IRF9. **e**, **f**, Similar to **a** and **b** but showing expression of p1@TRMT5 (housekeeping profile) and p2@TRMT5 (expressed in pathogen challenged monocytes). **g**, Histogram showing the number of different coexpression clusters (see Fig. 4) in which named genes with alternative promoters participate. The majority of genes with alternative promoters participate in more than one cluster; 17 genes participate in more than 10 different clusters and are not shown on this graph.

©2014 Macmillan Publishers Limited. All rights reserved

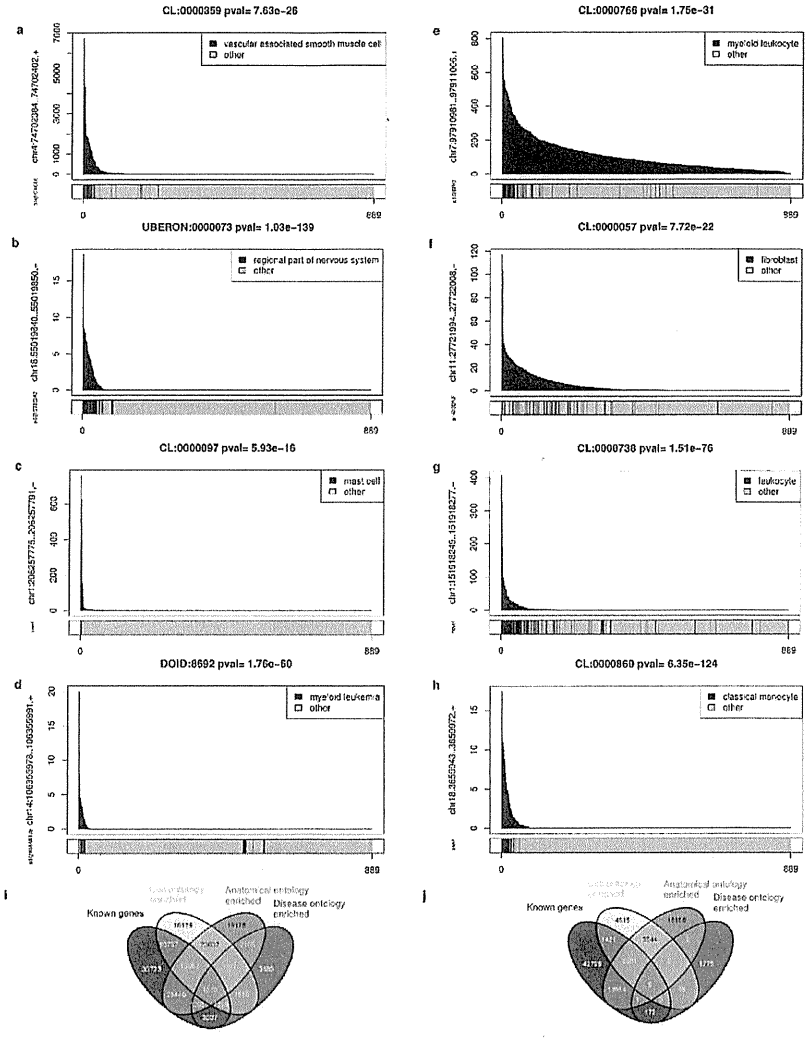

Extended Data Figure 11 | Sample ontology enrichment analysis (SOEA). Expression profile-sample ontology associations were tested by Mann–Whitney rank sum test to identify cell, disease or anatomical ontology terms over-represented in ranked lists of samples expressing each peak. **a**, p1@CXCL6 enriched in vascular associated smooth muscle cells. **b**, p5@ST8SIA3 enriched in brain tissues. **c**, Novel peak enriched in mast cells. **d**, p1@KIAA0125 enriched in myeloid leukaemia. **e**, p1@BRI3 enriched in myeloid leukaemia. **f**, p1@BDNF enriched in fibroblasts. **g**, Novel peak enriched in leukocytes. **h**, Novel peak enriched in classical monocytes. **i**, **j**, Venn diagrams showing degree of overlap between peaks associated to known genes (blue), cell ontology enriched (yellow), Uberon anatomical ontology enriched (green) and disease ontology (red). **i**, At a threshold of 10^{-20} (Mann–Whitney rank sum test), 64% (59,835 out of 93,558) of the expression profiles of human known transcripts and 74% (67,810 out of 91,269) of the expression profiles for novel transcripts show enrichment for one or more sample ontologies. **j**, Mouse sample ontology enrichment 10^{-20} threshold. 30% (18,273 out of 61,134) known are enriched and 47% (26,176 out of 55,143) novel are enriched.

©2014 Macmillan Publishers Limited. All rights reserved

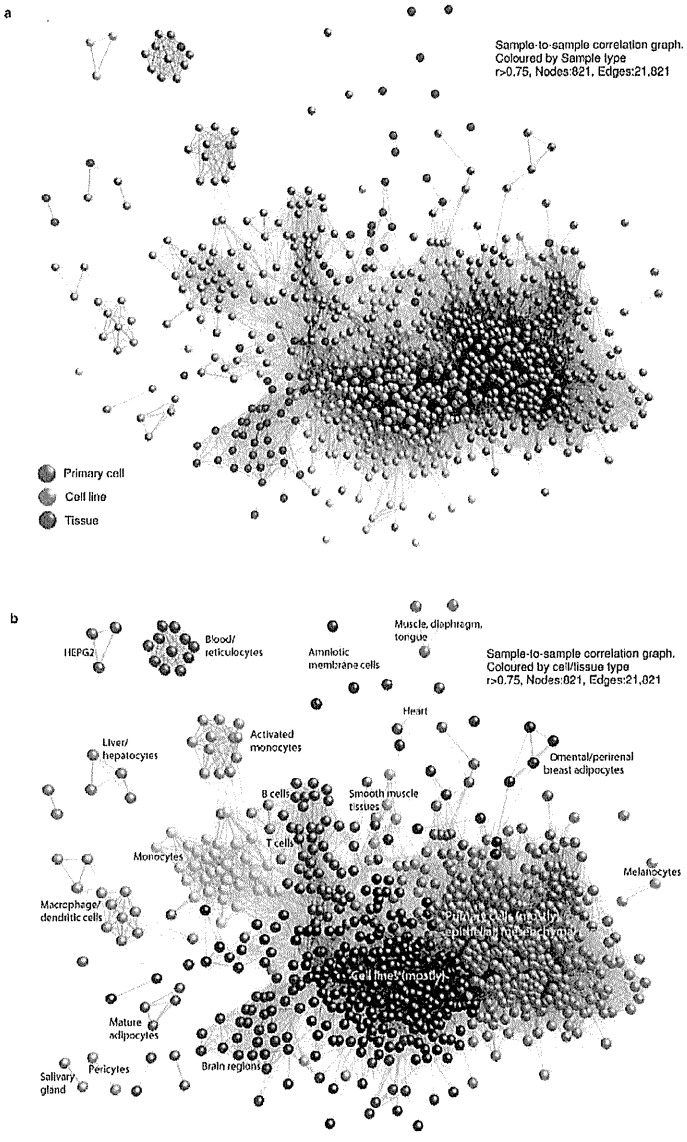

Extended Data Figure 12 | Sample-to-sample correlation graph. 821 nodes are shown, 21,821 edges shown ($r>0.75$). **a**, Samples are coloured by sample type (primary cell, cell line or tissue). Note the separation of cell lines and primary cells. **b**, As in **a**, except major subgroups are coloured and labelled separately.

©2014 Macmillan Publishers Limited. All rights reserved

IJBSCHS
[Original Article]

Biomedical Soft Computing and Human Sciences, Vol.18, No.2, pp.29-37
Copyright©1995 Biomedical Fuzzy Systems Association
(Accepted on 2011.2.1)

Effect of Music upon Awakening from Nap

Yuki TANAKA*, Hiroki NOGAWA** and Hiroshi TANAKA***

** Department of Medical Informatics, Tokyo Medical and Dental University Graduate School*
*** Fellowship Researcher, Japan Medical Information Network Associations*
**** Graduate School of Biomedical Science, Tokyo Medical and Dental University*

Abstract: *Sleep and awakening are critical issues for people under high levels of stress in modern society. However, only a few studies on the effects of music on awakening have been conducted; thus, we focused on the effect of music on comfortable awakening in humans. This paper is the first to analyze the comfort of forced awakening relative to music and the brain. This is an analytical and observational study: a descriptive study of awakening from naps with music using three psychological tests. Ten healthy subjects (5 men and 5 women) participated in this experiment. Quantitative analyses were conducted on the subjects' feelings when awakened from a nap either with music or with an alarm tone. The music changes with time: We change width of the frequency to output. Participants were awakened after naps of 30, 60, 90 and 120 minutes for a total of 8 times overnight. Subjective feelings just after awakening were measured with three psychological questionnaires. The differences between the subjective data with music and with an alarm tone were calculated and analyzed. The results indicate that awakening with music was more comfortable than awakening with an alarm tone. Additionally, differences in comfort levels between awakening with music and awakening with an alarm tone were smaller at 30 and 90 minutes than at 60 and 120 minutes, suggesting the effects of the circadian rhythms.*

Keywords *Awakening, Nap, Effect of Music, Circadian Rhythm, Sleep Rhythm*

1. Introduction

1.1 Research theme

This study is an initial step toward the goal of our research to quantify the response of a human when he/she hears music. Fig. 1 is a scheme of our research goal; first, we hypothesize the human as a black box with inputs and outputs, and then we analyze the human as a function of the inputs onto the outputs.

In this study, the input is music and the output is human subjective responses. Based on this scheme, we discuss comfortable awakening by music in this paper.

1.2 Background

Sleep and awakening are critical issues for people under high levels of stress in modern society. Many people work under circumstances in which they do not have good sleep conditions or they have to sleep against their circadian rhythms: for example, factory workers and healthcare workers who switch shifts or police officers or firefighters who work overnight. It is important to reduce physical fatigue through comfortable awakening to improve these job circumstances.

In this study, we performed quantitative analyses of the feelings that occur when awakened from a nap (short-term sleep). This paper is the first to analyze the

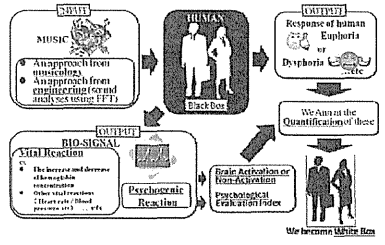

Fig. 1: Research goal

1-5-45 Yushima, Bunkyou-ku Tokyo, 113-8510, Japan,
Phone: +81-3-5803-4776 / Fax: +81-3-5803-0376
yukit@bioinfo.tmd.ac.jp

comfort of forced awakening relative to music and the brain.

1.3 Two Hypotheses

We propose two hypotheses regarding comfortable awakening. The first hypothesis states that awakening by music is more comfortable than awakening by only alarm tone sounds. The second hypothesis states that the comfort of awakening is determined by the sleep cycle and the circadian rhythm.

1.4 Conventional Research Details

Various studies on sleep have been conducted. Previous study was classified into eight different patterns according to their research themes.

The first research patterns focuses on the relation-ship between mortality and sleep time or sleep rhythm [1, 2]. Research in this area has found that the sleep length that causes the lowest mortality is 7 hours [1] and that mortality is high among those who are dissatisfied with the feeling of awakening [2]. The second research pattern measures the correlation between sleep rhythm and brain activity [3-7] using NIRS [3], polysomnography [4, 5], EEG [6] and blood pressure [7]. The third research pattern measures circadian rhythm [8] and concludes that circadian rhythm is related to the timing of REM sleep. The fourth research pattern examines the relationship between sleep and a physiological mechanism [9, 10], including a number of studies that focus on reduced leptin [9] or melatonin [10]. The fifth research pattern examines the physiological effect of naps or short-time sleep [11-16], measuring sleep characteristics using blood pressure [11, 12], modeling of the pattern of nap [13, 14], and investigating the relationship between naps and mortality [15, 16]. The sixth research pattern examines the sleep of sick patients or the relationship between the mortality of sick patients and sleep [17-21], including the effect of sleep on the mortality of insomnia or cancer patients [17, 18], the effect of sleep on memory in schizophrenia patients [19] and the sleep patterns of narcolepsy patients [20]. The seventh research pattern analyzes the effect of sleep quality on happiness in everyday life and on job performance [21-23], including measurements of sleepiness and its importance in everyday life [21] and the influence of sleep shortages [22, 23]. The final research pattern examines the influence of music on sleep [24, 25], including the efficacy of music for the initiation of sleep [24] and the excitatory effect of music on sleep [25]. Additionally, a number of studies investigate the psychological effect of music through non-invasive physiological measurements [26, 27]. Finally, some studies show that music affects the relaxation of stress [28].

We would like to emphasize that none of the pre-vious studies focused on awakening. Many of the pre-vious studies focused on "during sleep", "effect of sleep" or "initiations of sleep". However, only a few studies have been conducted on awakening from sleep, and none have been conducted on the effect of music on awakening..Given the lack of research in this area, we focus on comfortable awakening from sleep with music.

2. Method

2.1 Subject

The subjects were ten healthy Japanese volunteers: five men and five women. The average age was 28.3 (+-8.43) years. All of the subjects provided informed consent.

Table 1: Subjects

Subjects	Men	Women	Total
Number	5	5	10
Age	30.8±9.58	25.8±7.26	28.3±8.43

2.2 Questionnaries

We measured the subjective feelings of the subjects using three psychological questionnaires: the VAS (Visual Analogue Scale), the ALQ (Affective Level Questionnaire) and the POMS (Profile of Mood States). We chose three different types of tests because we did not want to trust only one psychological test, and we verified the reliability of each test.

A. VAS

Please indicate odor offensiveness upon awakening.

✧ How do you feel now? Please rate on a scale of one to ten. "5" is neutral.

	1	2	3	4	5	6	7	8	9	10	
Elation	○	○	○	○	○	○	○	○	○	○	Discomfort

B. ALQ

Are you feeling relaxed? or Are you feeling tense?

✧ Please choose the near feelings. "3" is neutral.

	1	2	3	4	5	
feeling of relaxation	○	○	○	○	○	Feeling of tense

C. POMS

Please choose the feeling that is closest to your current mood

Convivial mood

✧ Please choose the near feelings. "3" is neutral.

	1	2	3	4	5	
Great many	○	○	○	○	○	Strikingly absent

Fig.2: Samples of three questionnaires: (A) VAS, (B) ALQ and (C) POMS.

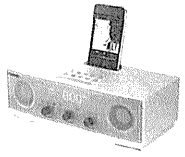

Fig. 3: Instrument

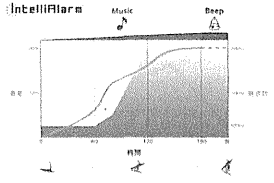

Fig. 4: Volume and Frequency band of *IntelliAlarm*

2.3 Use Instrument and Measurement Location

We used an *IntelliAlarm "TSX-80"* that is a product of YAMAHA Corporation (Fig. 3).

IntelliAlarm has 2 modes; (1) normal alarm mode using alarm tone sounds and (2) *IntelliAlarm* mode using music and alarm tone sounds. Figure 4 shows the distinctive features of *IntelliAlarm* mode, including volume and frequency. In *IntelliAlarm* mode, the volume of the sound source rises progressively starting three minutes before the preset time, and the alarm tone rings at the preset time.The frequency band rises progressively before the alarm tone sounds from 500 Hz to 20 kHz.

2.4 Musical pieces

We used jazz music from France because it would be unfamiliar to subjects. Subjects heard the music once before the start of the experiment. The reason using the jazz is because a base sounds being always played in one music.

2.5 Experiment environment

We prepared a private room for each subject. Every room was equipped with shading curtains to eliminate the effect of sunlight, as the experiment was conducted from 9:00 pm to 9:30 am. The *IntelliAlarm* was placed on the left side of the bed for each subject. Subjects turned off the light source in the room, except for the watery backlight of the *IntelliAlarm*.

2.6 Time protocol

We conformed to the following time protocol:

① Subjects were made awake with the IntelliAlarm mode (music and alarm tone sounds) or the normal alarm mode after naps lasting 30, 60, 90 and 120 minutes. The time schedule was randomized to ascertain whether the absolute timing in a day of sleep initiation and awakening influenced the response of the subjects.

② Subjects rested for 20 minutes following the nap to ensure that they were completely awake.

③ Subjects measured their subjective feelings during each rest time with psychological questionnaires. The psychological questionnaires were VAS, ALQ and POMS.

Some data are missing for subject number 3 due to trouble experimenting.

2.7 Calculation

To estimate the difference in subjective data for awakening with music and with an alarm tone, we defined the difference in the subjective data (ΔSD) as $\Delta SD = SD_{\text{awakening by music and alarm tone}} - SD_{\text{awakening by normal alarm}}$ for each test. In addition, we compared the average of all the questions in ΔSD of ALQ and the average for each attribute of questions in ΔSD of POMS.

We compared ΔSD awakening by music and alarm tone with ΔSD awakening by normal alarm tone sounds for each nap length with a t-test, and we examined the data for significant differences ($p<0.05$).

2.8 A hypothesis regarding awakening with music

We propose a hypothesis for a mechanism for the subject's responses to awakening with music.

Figure 5 shows a visual representation of our hypothesis. In Fig. 5, sound enters through our ears and is

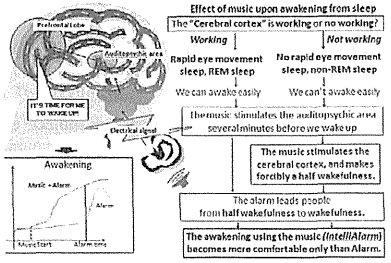

Fig. 5: A hypothesis for awakening by music

changed into corresponding electrical signals, which are first processed in the audiopsychic area and then in the prefrontal lobe, where we judge "It's time for me to wake up!" During this process, the comfort of awakening depends on whether the brain cortex is working (REM sleep) or not working (non-REM sleep). According to our hypothesis, the awakening effect of music should show better performance at the time of non-REM sleep than REM sleep. At the time of non-REM sleep, the music is assumed to stimulate cerebral cortex, and to make forced half awakening level resembling a state of REM sleep. After this half-awakening level is achieved, the alarm should lead people to wakefulness. According to this hypothesis, awakening by both music and alarm tone sounds should be more comfortable than with only normal alarm tone sounds.

3. Results

3.1 No time adjustment

Fig. 6, Fig. 7, and Fig. 8 show the relationship between nap length and ΔSD according to the three questionnaires.

Fig. 6 shows the result of ΔSD of VAS: the vertical axis representing the ΔSD and the horizontal axis representing nap length. In Fig. 6, awakening with music is more comfortable than awakening with an alarm tone, as ΔSD is positive. Additionally, in Fig. 6, ΔSD shows positive values for all nap lengths, with positive values of ΔSD being higher at 60 and 120 minutes than at 30 minutes and 90 minutes.

Fig.7 shows the result of ΔSD of ALQ: the vertical axis representing the ΔSD and the horizontal axis representing nap length. As shown in Fig. 7, awakening with music is more comfortable than awakening with an alarm

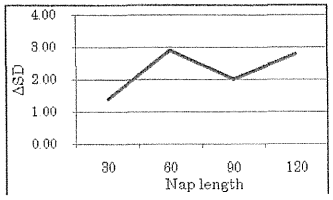

Fig. 6: ΔSD of VAS

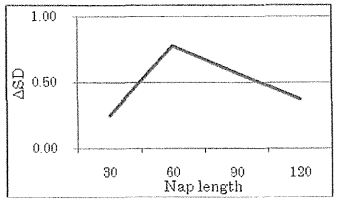

Fig. 7: ΔSD of ALQ

tone, as ΔSD is positive. Additionally, ΔSD shows positive values for all nap lengths, and ΔSD had the highest value at 60 minutes.

Figure 8 shows the results of ΔSD for POMS. Fig. 8(A) shows the results for the positive questions in POMS: the vertical axis representing ΔSD and the horizontal axis representing nap length. In Fig. 8(A), awakening with music is more comfortable than awakening

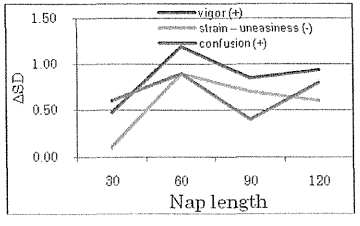

(A) Positive questions in POMS

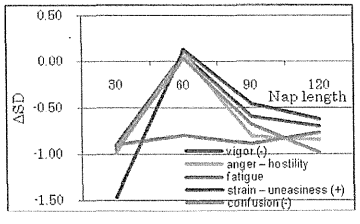

(B) Negative questions in POMS

Fig. 8: ΔSD of POMS

with an alarm tone, as ΔSD POMS $_{\text{positive question}}$ is positive. Fig. 8(B) shows the results for the negative questions in POMS: the vertical axis representing ΔSD and the horizontal axis representing nap length. In Fig. 8(B), awakening with music is more comfortable than awakening with an alarm tone, as ΔSD POMS $_{\text{negative question}}$ is negative. With regard to POMS positive questions (Fig. 8(A)), ΔSD had positive values for all nap lengths, and the positive values of ΔSD were highest at 60 and 120 minutes. With regard to POMS negative questions (Fig. 8(B)), ΔSD had negative values except at 60 minutes.

Table 2 shows the p values for the t-tests between nap length and the subjective data. We calculated p values using bilateral t-tests, assuming that each of the two groups was equally dispersed. With regard to VAS, we found significant differences ($p<0.05$) for all nap lengths, and greater significant differences ($p<0.005$) for 60 minutes and 120 minutes. The results of ALQ indicated significant differences for all nap lengths ($p<0.05$) except for 120 minutes. The results for the POMS indicated significant differences ($p<0.05$) for vigor (+) for all nap lengths.

Table 2: p values for nap length and subjective data

		30	60	90	120
	VAS	0.008	0.000	0.017	0.004
	ALQ	0.045	0.032	0.007	0.119
POMS	vigor (+)	0.044	0.006	0.002	0.005
POMS	vigor (-)	0.098	0.287	0.105	0.027
POMS	anger – hostility	0.110	0.313	0.016	0.034
POMS	fatigue	0.211	0.010	0.072	0.078
POMS	strain – uneasiness (+)	0.003	0.384	0.276	0.034
POMS	strain – uneasiness (-)	0.147	0.190	0.119	0.151
POMS	confusion (-)	0.105	0.328	0.126	0.002
POMS	confusion (+)	0.110	0.180	0.324	0.115

* The filled cells represent $p<0.05$

3.2 Adjustment by the time (Data analysis except data from 3:00 am to 5:00 pm

An analysis of questionnaires between 3:00 am and 5:00 am found that all subjects reported negative feelings. Therefore, we performed a data adjustment to exclude the data during this time period. Figure 9, Figure 10, and Figure 11 show ΔSD for the 3 questionnaires excluding data from 3:00 am till 5:00 am.

Fig. 9 shows the results of ΔSD of VAS, with the vertical axis representing ΔSD and the horizontal axis

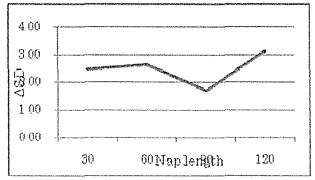

Fig. 9: ΔSD of VAS excluding 3:00 am until 5:00 am data

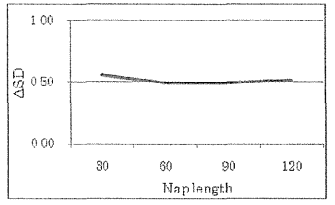

Fig. 10: ΔSD of ALQ excluding 3:00 am until 5:00 am data

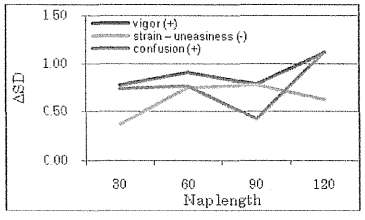

(A) Positive questions in POMS

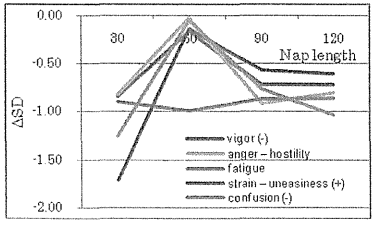

(B) Negative questions in POMS

Fig. 11: ΔSD of POMS excluding 3:00 am until 5:00 am data

representing nap length. Awakening with music is more comfortable than with alarm tones, as ΔSD is positive. Additionally, ΔSD is positive for all nap lengths, and the positive values of ΔSD are highest at 60 and 120 minutes.

Fig. 10 shows the results of ΔSD of ALQ excluding 3:00 am until 5:00 am data: the vertical axis representing ΔSD and the horizontal axis representing nap length.

Awakening with music is more comfortable than with alarm tones, as ΔSD is positive. ΔSD is positive for all nap lengths.

Fig. 11 shows the results of ΔSD of POMS excluding 3:00 am until 5:00 am data: the vertical axis representing ΔSD and the horizontal axis representing nap length. Fig. 11(A) shows the results for the positive questions in the POMS. Awakening with music is more comfortable than with alarm tones, as ΔSD is positive. Fig. 11(B) shows the results for the negative questions in the POMS. Awakening with music is more comfortable than with alarm tones, as ΔSD for negative questions is negative. The results for the POMS $_{\text{positive questions}}$ shows that ΔSD is positive for all nap lengths, and the positive values of ΔSD are highest at 60 and 120 minutes.

Table 3 shows the p values for the t-tests between nap length and the subjective data We calculated p values using bilateral t-tests, assuming that each of the two groups were not equally dispersed because some data revealed a significant bias.

Table 3: p values for nap length and subjective data excluding 3:00 am till 5:00 am data

		30	60	90	120
VAS		0.011	0.000	0.028	0.001
ALQ		0.083	0.044	0.013	0.023
POMS	vigor (+)	0.092	0.002	0.003	0.003
	vigor (-)	0.028	0.329	0.036	0.024
	anger – hostility	0.064	0.468	0.007	0.040
	fatigue	0.098	0.033	0.056	0.053
	strain – uneasiness (+)	0.001	0.341	0.114	0.030
	strain – uneasiness (-)	0.184	0.057	0.051	0.115
	confusion (-)	0.005	0.449	0.062	0.003
	confusion (+)	0.196	0.079	0.172	0.022

* The filled cells represent p<0.05

The results of VAS indicate significant differences (p<0.05) for all nap lengths, and greater significant differences (p<0.005) were found at 60 minutes and 120 minutes. Comparisons between the raw data in Fig. 6 and the adjusted data in Fig. 9 for all nap lengths revealed that ΔSD of adjusted data decreased for the 90 minute length and increased for the 30 minute length in the adjusted data as compared to the raw data. The results of ALQ indicate significant differences (p<0.05) for all nap lengths. Comparisons between the raw data in Fig. 7 and the adjusted data in Fig. 10 revealed that ΔSD of ALQ fluctuated less in the adjusted data. The result of POMS showed number of time which shows significant difference (p<0.05) at vigor (-) increases compared with corresponding rows in Tables 2.

4. Discussion

The results of ΔSD show that awakening by music was more comfortable than awakening by alarm tone sounds for all nap lengths, except in the POMS $_{\text{negative questions}}$ in the raw data for the 60 minute nap length. Given this finding, we conclude that awakening with music is more comfortable than awakening with alarm tone sounds.

The difference of comfort between awakening with music and awakening with alarm tone sounds was smaller at 30 and 90 minutes than at 60 and 120 minutes, except for POMS negative questions in both the raw and adjusted data and also for the ALQ in the adjusted data. We presume this phenomenon is caused by sleep cycles, in which humans are in REM sleep states at 90 minutes and in non-REM sleep states at 30 minutes, because the past studies prove that the stage of the sleep changes with time and REM occur every 90 minutes [6].

The results of POMS show contradictions between the POMS $_{\text{positive questions}}$ and the POM$_{\text{S negative questions}}$ at the 60 minute nap length. We assume that this contradiction is caused by the confused consciousness of the subjects, causing a lower increase of consciousness at this time due to human sleep cycles: humans are in non-REM sleep state at 60 minutes, because the past studies prove that the stage of the sleep changes with time and around the sleep of 60 minutes is shallow stage of sleep [6]. In this study, we supported that the clear fact that the feelings of awakening depend on a stage of the sleep in past studies [29] and an everyday sense.

Exclusion of the data from 3:00 am until 5:00 am strengthened the significant differences between music and alarm tones. This result reveals that subjects felt negative when awakened in the 3:00 am until the 5:00 am window, regardless of the presence of music. We speculate that this negative feeling was caused by the circadian rhythm.

In addition, we think about the future prospects as follows. By this experiment, we think that we have to compare subjectivity data at awakening with objectivity data of the depth of the sleep, and we think that we have to increase the subjects. In this experiment, we considered the psychology experimental data by support of past studies, but we think our study have to be backed up by objective data. And we provided jazz music for the reason of base sounds being always played in one music at this experiment, but we think that we have to pursue optimal "music" at awakening. Moreover, we experimented on the awakening from a nap at this experiment, but we think that we have to experiment the awakening from normal sleep.

5. Conclusion

In this paper, we discussed comfortable awakening with music because comfortable awakening is a critical issue for people under high levels of stress. We proposed a mechanism for comfortable awakening with music that is irrelevant of the stage of sleep. We assume that music stimulates the cerebral cortex and forces a half-awake level that resembles a state of REM sleep during non-REM sleep. We measured the subjective feelings of 10 healthy volunteers using 3 psychological questionnaires: the VAS, ALQ and POMS. The results suggest the following 3 conclusions: (A) awakening with music is more comfortable than awakening with alarm tone sounds because ΔSD (the difference in the subjective data between awakening by music accompanied by an alarm tone and awakening with only the normal alarm tone) is positive in almost every questionnaire; (B) sleep rhythm causes confused consciousness in subjects because ΔSD for the POMS showed contradictions between the POMS$_{\text{positive questions}}$ and the POMS$_{\text{negative questions}}$ for the 60 minute nap length in the non-REM sleep state; and (C) circadian rhythm affects awakening comfort, as the subjects reported feeling negative from 3:00 am until 5:00 am regardless of the presence of music.

In conclusion, we summarize our results as follows:

1) Awakening by music feels more comfortable.
2) Sleep rhythm and the circadian rhythm influence awakening comfort.

Acknowledgements

This study was done under contribution of Yamaha Corporation. The authors are grateful to Mr. Daiki KURAMITSU and Mr. Yasuhiko ASAHI of Desktop Audio Group in Yamaha Corporation for assistance with experiments. Finally we thank all volunteers.

References

[1] Tamakoshi,A., Ohno,Y.: Self-reported sleep duration as a predictor of all-cause mortality: results from the JACC study, Japan, SLEE, No.27 Vol.1, pp.51-54, 2004

[2] Kojima,M., Wakai,K., Kawamura,T., Tamakoshi,A., Aoki,R., Lin,Y., Nakayama,T., Horibe,H., Aoki,N., Ohno,Y.: Sleep patterns and total mortality: a 12-year follow-up study in Japan, Journal of Epidemiology, No.10 Vol.2, pp.87-93, 2000

[3] Mariko,I., Yoshikata,A., Kazumi,T., Shinichi,S., Hideto,H., Ryousei,Y., Atsushi,M., Yuichi,Y., Hideaki,K.: Activation of visual cortex in REM sleep measured by 24-channel NIRS imaging, Psychiatry and Clinical Neurosciences, No.55, pp.187–188, 2001

[4] P,L,Madsen., J,F,Schmidt., G,Wildschiodtz., L,Friberg., S,Holm., S,Vorstrup., N,A,Lassen.: Cerebral O2 metabolism and cerebral blood flow in humans during deep and rapid-eye-movement sleep, Journal of Applied Physiology, No.70, pp.2597-2601, 1991

[5] Takahashi,K., Atsumi,Y.: Precise measurement of individual rapid eye movements in REM sleep of humans, SLEEP, No.20 Vol.9: 743-52, 1997

[6] W,Dement.: Cyclic variation in EEG during sleep and their relation to eye movements, body motility and dreaming. Electroencephalography and Clinical Neurophysiology, No.9 Vol.4, pp.673-690, 1957

[7] Frederick,S., J,Allan,H., Donald,F,M., Frederick,G.: Changes in respiration heart rate and systolic blood pressure in human sleep, Journal Applied Physiology, No.19, pp.417-422, 1964

[8] Czeisler,CA., Zimmerman,JC., Ronda,JM., Moore-Ede,MC., Weitzman,ED.: Timing of REM sleep is coupled to the circadian rhythm of body temperature in man, SLEEP, No.2 Vol.3, pp.329-46, 1980

[9] Shahrad,T., Ling,L., Diane,A., Terry,Y., Emmanuel,M.: Short sleep duration is associated with reduced leptin, elevated ghrelin, and increased body mass index, PLoS MEDICIN, No.1 Vol.3, pp.210-217, 2004

[10] Tali,G., Yaniv,A., Yonatan,G., Yaara,Y., Nava,Z.: Sleep-anticipating effects of melatonin in the human brain. NeuroImage, No.31, pp.410- 418, 2006

[11] Stergiou,GS., Malakos,JS., Zourbaki,AS., Achimastos,AD., Mountokalakis,TD.: Blood pres-

sure during siesta: effect on 24-h ambulatory blood pressure profiles analysis. Journal of Human Hypertension, No.11 Vol.2, pp.125-31, 1997

[12] Stergiou,GS., Mastorantonakis,SE., Roussias, LG.: Intraindividual reproducibility of blood pressure surge upon rising after nighttime sleep and siesta. Hypertension Researc, No.31 Vol.10, pp.1859-64, 2008

[13] Frederik,B,. Marc,J,. Hartmut,S.: Modeling Napping, Post-Lunch Dip, and Other Variations in Human Sleep Propensity, SLEEP, No.32 Vol.3, pp.392-398, 2009

[14] Emmanouil,P., Thomas,N., Michail,N., Ourania,S., Maria,B., Emmanouil,G.: Siesta and sleep patterns in a sample of adolescents in Greece. Pediatrics International, No.50, pp.690–693, 2008

[15] Bursztyn,M., Stessman,J.:The Siesta and Mortality: Twelve years of prospective observations in 70-year-olds, SLEEP, No.28 Vol.3, pp.298-299, 2005

[16] Androniki,N., Eleni,O., Antonia,T., Theodora,P., Dimitrios,T.: Siesta in Healthy Adults and Coronary Mortality in the General Populatio, Archives of Internal Medicine, No.167, pp.296-301, 2007

[17] Kripke,DF., Garfinkel,L., Wingard,DL., Klauber,MR., Marler,MR.: Mortality Associated With Sleep Duration and Insomnia, Archives of General Psychiatry, No.59, pp.131-136, 2002

[18] Kripke,DF., Simons,RN., Garfinkel,L., Hammond,EC.: Short and long sleep and sleeping pills. Is increased mortality associated?, Archives of General Psychiatry, No.36 Vol.1, pp.103-16, 1979

[19] Mareen,S H., Paul,C B., Serap,S., Andrea,B., Josef,B A., Robert,G.: Effects of daytime naps on procedural and declarative memory in patients with schizophrenia, Journal of Psychiatric Research, No.44 Vol.1, pp.42-47, 2010

[20] Nobili,L., Ferrillo,F., Besset,A., Rosadini,G., Schiavi,G., Billiard,M.: Ultradian aspects of sleep in narcolepsy, Neurophysiologie Clinique, No.26 Vol.1, pp.51-9, 1996

[21] SIGNAL,T L., GANDER,P H., ANDERSON,H., BRASH,S.: Scheduled napping as a countermeasure to sleepiness in air traffic controllers, Journal of Sleep Research, No.18, pp.11–19, 2009

[22] Iris,A., Catherine,S F., Eva,L., Laura,C., Sally,B., John,W.: How is good and poor sleep in older adults and college students related to daytime sleepiness, fatigue, and ability to concentrate?, Journal of Psychosomatic Research, No.49, pp.381-390, 2000

[23] Carskadon, M A.: Patterns of sleep and sleepiness in adolescents, Pediatrician, No.17 Vol.1, pp.5-12, 1990

[24] Johnson, JE.: The use of music to promote sleep in older women, Journal of Community Health Nursing, No.20 Vol.1, pp.27-35, 2003

[25] Michael,H B., Donna, L A.: The impact of music upon sleep tendency as measured by the multiple sleep latency test and maintenance of wakefulness test, Physiology & Behavior, No.71, pp.485 – 492, 2000

[26] WATANABE,S., YAO, F., TAKAUE, R.: Fundamental Study on Effects of Listening of Wind Band Music to the Changes of Blood Pressure and Heart Rate in Daily Living Environment, Biomedical Soft Computing and Human Sciences, No.12 Vol.1, pp.9-15, 2007

[27] Michael, S., Alex,P.: Stress and Lie Detection through Non-Invasive Physiological Sensing, Biomedical Soft Computing and Human Sciences, Vol.14 No.2,pp.109-116, 2009

[28] Pelletier,CL.: The effect of music on decreasing arousal due to stress: a meta-analysis, Journal of music therapy, No.41 Vol.3, pp.192-214, 2004

[29] Koki, M., Yaso, M., Tsujimura, S., Yunokuchi, K.: Real-time measurement on Detection of REM sleep using the instantaneous heart beat, The Institute of Electronics, Information and Communication Engineers, Vol.104 Mo.644, pp.45-48, 2005

Yuki TANAKA

She received a Bachelor of Engineering degree from Tokai University, Japan, in 2005, and a Master of Engineering from Tokai University, Japan, in 2007. Since April 2007, she has been a Ph.D. student at Tokyo Medical and Dental University Graduate School, Department of Medical Informatics.

She studied piano in Japan under the pianist Toshie Nakashima since 1985, beginning when she was 4 years old. She has participated in piano contests and she has received several prizes.

She is a part-time teacher at Nippon University (from 2008) and Kitasato University (from 2007). Her current research interests are "Music therapy for dementia patients: Tuned for culture differences" and the "Effect of music upon awakening for comfortable awakening."

Hiroki NOGAWA

He graduated from Osaka University Medical School and received his Medical License in 1990.

He worked as a surgical resident at Osaka University Hospital from June 1990 to June 1991 and at Kure National Hospital from July 1991 to June 1993. He received a doctorate in Internal Medicine from Osaka University in 1997. He was an Assistant Professor at Sapporo Medical School from April 1997 to June 1999 and a Lecturer at Sapporo Medical School from July 1999 to July 2000. He was a Lecturer in the Cybermedia Center at Osaka University from August 2000 to June 2004 and a Visiting Professor at Tokyo Medical and Dental University from August 2004 to July 2008. Since August 2008, he has been a Fellowship Researcher at the Japanese Medical Information Network Association. His current research interests are internet security tech-nology, public policy on information and communication technologies (including medical informatics), socio-legal and technological issues (including copyright issues), and the physiological effects of music on the brain.

Hiroshi TANAKA

Hiroshi Tanaka was born in Tokyo, Japan in 1949. He received a Bachelor of Engineering degree from The University of Tokyo, Japan, in 1974 and a Master of Engineering degree from the Graduate School of Engineering, The University of Tokyo, Japan, in 1976. He received a Doctor in Medical Science degree from the Graduate School of Medicine, The University of Tokyo, Japan, in 1981 and a Ph.D. from the Graduate School of Engineering, The University of Tokyo, Japan, in 1983.

He was an Assistant Professor at the Institute for Medical Electronics in the School of Medicine of The University of Tokyo from 1982 to 1987, a Visiting Scientist at Uppsala University and Linkoping University in Sweden from 1982 to 1984, an Associate Professor at Hamamatsu University School of Med-icine from 1987 to 1991, and a Visiting Scientist in the MIT Laboratory of Computer Science in 1990. He became a Full Professor of Bioinformatics at Tokyo Medical and Dental University in 1991 and has been the Dean of the Biomedical Science PhD Program of Tokyo Medical and Dental University since 2006. His current research interests are medical informatics, systems biology, systems pathology, and clinical bioinformatics.

nature COMMUNICATIONS

ARTICLE

Received 20 Aug 2013 | Accepted 30 Sep 2013 | Published 5 Nov 2013

DOI: 10.1038/ncomms3686

Mepenzolate bromide displays beneficial effects in a mouse model of chronic obstructive pulmonary disease

Ken-Ichiro Tanaka[1], Tomoaki Ishihara[1], Toshifumi Sugizaki[1], Daisuke Kobayashi[1], Yasunobu Yamashita[1], Kayoko Tahara[1], Naoki Yamakawa[1], Kumiko Iijima[2], Kaoru Mogushi[2], Hiroshi Tanaka[2], Keizo Sato[3], Hidekazu Suzuki[4] & Tohru Mizushima[1]

The clinical treatment of chronic obstructive pulmonary disease (COPD) requires not only an improvement of airflow by bronchodilation but also the suppression of emphysema by controlling inflammation. Here we screen a compound library consisting of clinically used drugs for their ability to prevent elastase-induced airspace enlargement in mice. We show that intratracheal administration or inhalation of mepenzolate bromide, a muscarinic antagonist used to treat gastrointestinal disorders, decreases the severity of elastase-induced airspace enlargement and respiratory dysfunction. Although mepenzolate bromide shows bronchodilatory activity, most other muscarinic antagonists do not improve elastase-induced pulmonary disorders. Apart from suppressing elastase-induced pulmonary inflammatory responses and the production of superoxide anions, mepenzolate bromide reduces the level of cigarette smoke-induced airspace enlargement and respiratory dysfunction. Based on these results, we propose that mepenzolate bromide may be an effective therapeutic for the treatment of COPD due to its anti-inflammatory and bronchodilatory activities.

[1] Department of Analytical Chemistry, Faculty of Pharmacy, Keio University, 1-5-30, Shibakoen, Minato-ku, Tokyo 105 8512, Japan. [2] Division of Medical Genomics, Department of Bioinformatics, Medical Research Institute, Tokyo Medical and Dental University, 1-5-45, Yushima, Bunkyo-ku, Tokyo 113 8510, Japan. [3] Kyushu University of Health and Welfare, 1714-1, Yoshino-cho, Nobeoka 882 8508, Japan. [4] Division of Gastroenterology and Hepatology, Department of Internal Medicine, Keio University School of Medicine, 35, Shinanomachi, Shinjuku-ku, Tokyo 160 8582, Japan. Correspondence and requests for materials should be addressed to T.M. (email: mizushima-th@pha.keio.ac.jp).

© 2013 Macmillan Publishers Limited. All rights reserved.

Chronic obstructive pulmonary disease (COPD) is a serious health problem whose most important etiologic factor is cigarette smoke (CS)[1]. COPD is a disease that is defined by a progressive and partially reversible airflow limitation associated with abnormal inflammatory responses and permanent enlargement of the pulmonary airspace[1–3]. Thus, for the clinical treatment of COPD, it is important not only to improve the airflow limitation by bronchodilation, but also to suppress disease progression by controlling inflammatory processes.

Bronchodilators (β_2-agonists and muscarinic antagonists) are currently used for the treatment of COPD, providing an effective temporary improvement of airflow limitation[2,4,5]. On the other hand, steroids are used to suppress the inflammatory responses associated with COPD. However, steroids cannot significantly modulate disease progression and mortality[5,6] because the inflammation associated with COPD shows resistance to steroid treatment[7].

In addition to the fact that CS contains a high concentration of reactive oxygen species (ROS), activated leukocytes also produce large amounts of ROS, with one such example being the superoxide anions produced *via* the activation of nicotinamide adenine dinucleotide phosphate (NADPH) oxidase[8]. In contrast to this, the body contains a number of endogenous antioxidant proteins such as superoxide dismutase (SOD) and glutathione *S*-transferase (GST), with a decrease in these proteins reported to be involved in the pathogenesis of COPD[9,10]. The inflammatory responses associated with COPD are thought to be triggered by oxidative stress and mediated through the activation of nuclear factor-κB (NF-κB, a pro-inflammatory transcription factor) and inhibition of histone deacetylase 2 (HDAC2)[11–14]. Oxidative stress seems to activate NF-κB through the inhibition of HDAC activity and degradation of inhibitor of NF-κB (IκB)-α (refs 12,14,15). Pro-inflammatory gene expression is normally silenced by the condensation of DNA; however, the acetylation of core histones opens up the condensed chromatin and induces the expression of these genes (refs 11,12,16). HDACs suppress the expression of pro-inflammatory genes not only by maintaining chromatin condensation but also by directly modifying pro-inflammatory transcription factors (such as NF-κB)[12]. Moreover, HDACs, and particularly HDAC2, seem to have important roles in the inflammatory responses associated with COPD[11,17,18]. Furthermore, because corticosteroids use HDAC2 to suppress the activity of NF-κB[11,12,19], the inhibitory effect of CS on HDAC2 may be responsible for the reduced sensitivity of COPD patients to steroid treatment[11]. Therefore, compounds that activate HDAC2 or inhibit ROS production and NF-κB may be effective for the treatment of inflammation associated with COPD.

In the present study, we screen compounds that prevent elastase-induced airspace enlargement in mice from a library of existing medicines whose safety properties have already been well characterized in humans. We select mepenzolate bromide (mepenzolate), which is an orally administered muscarinic receptor antagonist used to treat gastrointestinal disorders[20–22], and administer this compound to mice, which suppresses elastase-induced pulmonary inflammatory responses, airspace enlargement, alteration of lung mechanics and respiratory dysfunction. We also found that mepenzolate has bronchodilatory activity. These results suggest that mepenzolate achieves its anti-inflammatory effect *via* muscarinic receptor-independent inhibitory effects on NF-κB and NADPH oxidase, together with stimulatory effects on HDAC2, SOD and GST. We suggest that mepenzolate could provide an effective treatment option for COPD, not only as a consequence of its bronchodilatory activity but also due to its anti-inflammatory properties.

Results

Effect of mepenzolate on airspace enlargement. From a group of 83 medicines already in clinical use (Supplementary Table S1), we screened for compounds able to suppress porcine pancreatic elastase (PPE)-induced airspace enlargement. Each drug was administered intraperitoneally to mice, and after selecting eight candidate compounds based on the level of suppression of airspace enlargement (Supplementary Table S1), these were administered intratracheally at various doses and their inhibitory effects on PPE-induced airspace enlargement evaluated. Following this process, mepenzolate was selected based on the level of suppression of airspace enlargement it provided at clinical dose or less.

Histopathological analysis of pulmonary tissue using hematoxylin and eosin (H&E) staining revealed that PPE administration induced airspace enlargement (increase in the mean linear intercept (MLI)) and that the simultaneous daily intratracheal administration of mepenzolate suppressed this enlargement in a dose-dependent manner (Fig. 1a,b).

The alteration of lung mechanics associated with pulmonary emphysema is characterized by a decrease in elastance. Total respiratory system elastance (elastance of the whole lung, including the bronchi, bronchioles and alveoli) and tissue elastance (elastance of alveoli) were decreased by the PPE treatment in a manner that could be restored in part by the simultaneous administration of mepenzolate, again in a dose-dependent manner (Fig. 1c).

We next examined the effect of mepenzolate administered by the inhalation route on the PPE-induced airspace enlargement and alteration of lung mechanics. The results obtained (Fig. 1d–f) were similar to those observed with the intratracheal mode of administration (Fig. 1a–c).

To determine the effect of mepenzolate on pre-developed pulmonary emphysema, the intratracheal administration of mepenzolate to mice was commenced 14 days after the administration of PPE, and airspace enlargement and lung mechanics were assessed on day 21. Compared with vehicle-treated animals, mepenzolate decreased the extent of PPE-induced airspace enlargement and alterations to lung mechanics (Fig. 2a–c), suggesting that mepenzolate could be an effective compound for the treatment of pre-developed pulmonary emphysema.

Effects of other muscarinic antagonists. We next examined the effects of other muscarinic antagonists on PPE-induced airspace enlargement and alterations of lung mechanics. Even at the highest dose, none of muscarinic antagonists tested significantly suppressed the PPE-induced airspace enlargement or alterations in lung mechanics (Fig. 3a–c).

The diagnosis of COPD is confirmed by a decrease in the ratio of forced expiratory volume in the first second (FEV_1) to forced vital capacity (FVC)[1]. We recently established a technique to monitor PPE-induced respiratory dysfunction in mice, and found that the $FEV_{0.05}$/FVC ratio clearly decreased in PPE-treated mice compared with control mice[23]. Using this technique, we examined here the effects of mepenzolate and other muscarinic antagonists on the PPE-induced decrease in $FEV_{0.05}$/FVC. To washout the bronchodilatory effect of the muscarinic antagonists, the administration of each drug was discontinued on day 10 and the assay performed on day 14. PPE treatment decreased the $FEV_{0.05}$/FVC ratio, whereas the simultaneous administration of mepenzolate, but not the other muscarinic antagonists, restored the $FEV_{0.05}$/FVC towards control values (Fig. 3d). The results in Fig. 3 show that ipratropium bromide (ipratropium), scopolamine *N*-butylbromide (scopolamine) and pirenzepine

© 2013 Macmillan Publishers Limited. All rights reserved.

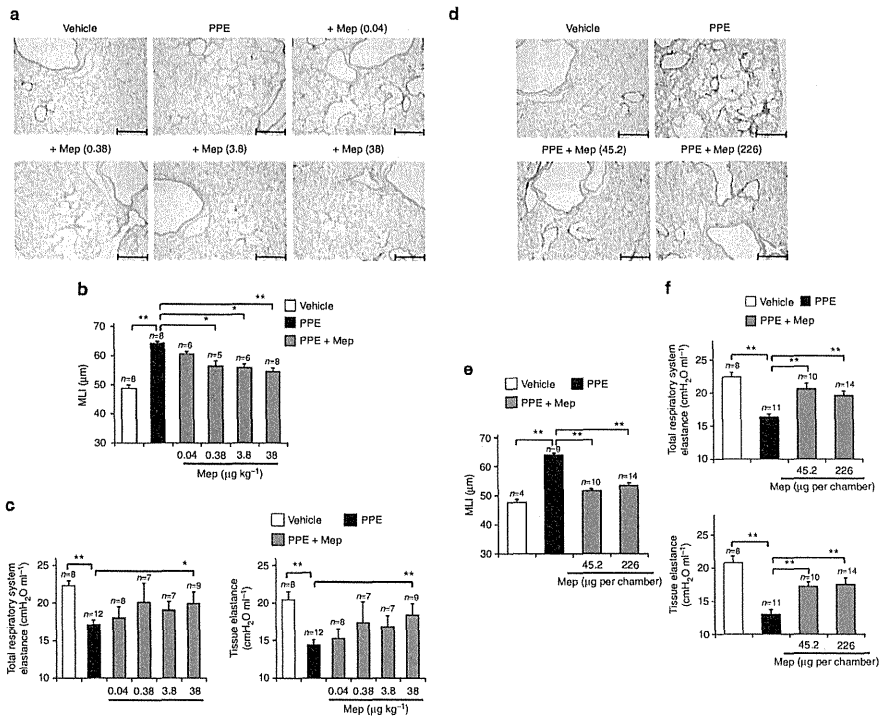

Figure 1 | Effect of mepenzolate on PPE-induced pulmonary disorders. Mice were treated with PPE (100 μg per mouse) once only on day 0 or with the vehicle only. The indicated doses (**a**–**c**, μg kg^{-1}; **d**–**f**, μg per chamber) of mepenzolate (Mep) were administered intratracheally (**a**–**c**) or by inhalation (**d**–**f**) once daily for 14 days (from day 0 to day 13). Sections of pulmonary tissue were prepared on day 14 and subjected to histopathological examination (H&E staining) (scale bar, 500 μm) (**a**,**d**). Airspace size was estimated by determining the MLI as described in the Materials and Methods (**b**,**e**). Total respiratory system elastance and tissue elastance were determined on day 14 as described in the Methods (**c**,**f**). Values represent the mean ± s.e.m. $^{*}P<0.05$; $^{**}P<0.01$ (Tukey test). Experiments were replicated at least two times.

dihydrochloride (pirenzepine) were not effective in combatting PPE-induced airspace enlargement, nor did they improve lung mechanics or respiratory dysfunction. This finding suggests that mepenzolate achieves its ameliorative effect over PPE-induced pulmonary disorders *via* mechanisms that are independent of its effects on muscarinic receptors and bronchodilatory activity.

To further test this idea, we examined the bronchodilatory activity induced by the muscarinic antagonists mentioned above. As shown in Fig. 4a, the dose-dependent increase in airway resistance (bronchoconstriction) induced by inhaled methacholine was completely suppressed by the intratracheal pre-administration of mepenzolate, thus attesting to the latter's bronchodilatory activity. The dose-response profile of ipratropium for bronchodilation was similar to that of mepenzolate (Fig. 4a), although ipratropium had no effect against the PPE-induced pulmonary disorders (Fig. 3). Neither scopolamine nor pirenzepine showed bronchodilatory activity, at least not at the highest dose employed here (Supplementary Fig. S1). These results further support the notion that mepenzolate achieves its ameliorative effect against PPE-induced pulmonary disorders *via* muscarinic receptor- and bronchodilatory activity-independent mechanisms. In addition, the results in Fig. 4b show that, as for ipratropium, the bronchodilatory activity of mepenzolate was transient, diminishing 48 h after its administration.

Muscarinic antagonists used to treat COPD are categorized as being long acting (such as tiotropium bromide (tiotropium) and glycopyrronium bromide (glycopyrronium)) or short acting (such as ipratropium), with the long-acting muscarinic antagonists now considered the standard bronchodilator treatment for COPD[24]. We subsequently examined the effect of intratracheal administration of tiotropium or glycopyrronium on PPE-induced pulmonary disorders. As shown in Supplementary Fig. S2a–c, glycopyrronium suppressed the PPE-induced airspace enlargement and alterations of lung mechanics. However, the extent of amelioration of airspace enlargement was not as apparent as that seen with mepenzolate (Supplementary Fig. S2b), and glycopyrronium did not significantly suppress the PPE-induced respiratory dysfunction (Supplementary Fig. S2d).

© 2013 Macmillan Publishers Limited. All rights reserved.

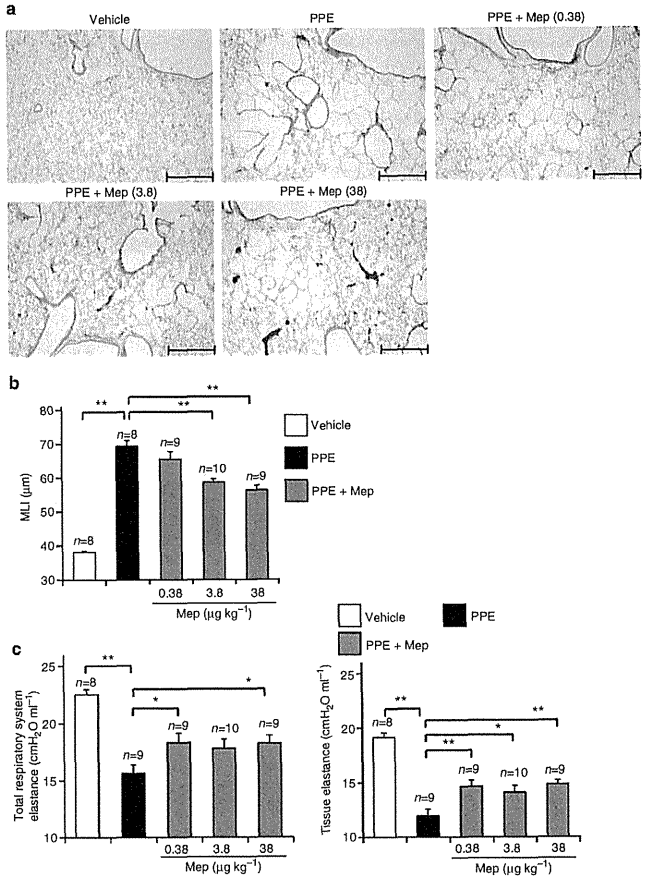

Figure 2 | Effect of mepenzolate on pre-developed pulmonary emphysema. Mice were treated with PPE (100 μg per mouse) once only on day 0 or with the vehicle only. The indicated doses (μg kg^{-1}) of mepenzolate (Mep) were administered intratracheally once daily from day 14 to day 20. Sections of pulmonary tissue were prepared on day 21 and subjected to histopathological examination (H&E staining) (scale bar, 500 μm) (**a**). Airspace size was estimated by determining the MLI as described in the Materials and Methods (**b**). Total respiratory system elastance and tissue elastance were determined on day 21 as described in the Methods (**c**). Values represent the mean ± s.e.m. $^{*}P<0.05$; $^{**}P<0.01$ (Tukey test). Experiments were replicated at least two times.

On the other hand, tiotropium did not suppress the PPE-induced airspace enlargement, alterations of lung mechanics or respiratory dysfunction (except for a weak suppression of tissue elastance at the 30 μg kg^{-1} dose) (Supplementary Fig. S2a–d).

Effect of mepenzolate on inflammatory responses. We next monitored PPE-induced pulmonary inflammatory responses by determining the number of leucocytes in bronchoalveolar lavage fluid (BALF) 24 h after the administration of PPE. As shown in Fig. 5a, the total number of leucocytes and individual number of neutrophils were increased by the PPE treatment and this effect was suppressed by the simultaneous administration of mepenzolate. We also examined the levels of pro-inflammatory cytokines (tumour necrosis factor-α) and chemokines (macrophage inflammatory protein-2, monocyte chemoattractant protein-1 and keratinocyte-derived chemokine) in BALF. Levels of these pro-inflammatory cytokines and chemokines increased after the PPE treatment, and this increase was suppressed by the simultaneous treatment of animals with mepenzolate (Fig. 5b). These

© 2013 Macmillan Publishers Limited. All rights reserved.

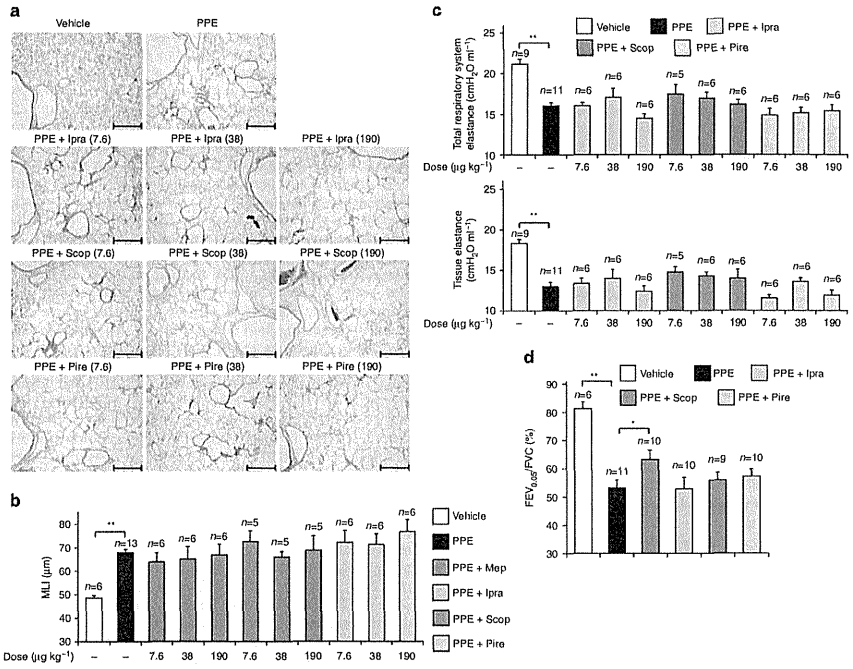

Figure 3 | Effect of different muscarinic antagonists on PPE-induced pulmonary disorders. Mice were treated with PPE (100 μg per mouse) once only on day 0 or with the vehicle only. The indicated doses (μg kg^{-1}) (**a–c**) or 38 μg kg^{-1} (**d**) of ipratropium (Ipra) (**a–d**), scopolamine (Scop) (**a–d**), pirenzepine (Pire) (**a–d**) or mepenzolate (Mep) (**d**) were administered intratracheally once daily for 14 days (from day 0 to day 13) (**a–c**) or for 11 days (from day 0 to day 10) (**d**). Sections of pulmonary tissue were prepared on day 14 and subjected to histopathological examination (H&E staining) (scale bar, 500 μm) (a). Airspace size was estimated by determining the MLI as described in the Materials and Methods (**b**). Total respiratory system elastance and tissue elastance were determined on day 14 as described in the Methods (**c**). The $FEV_{0.05}$/FVC was determined on day 14 as described in the Materials and Methods (**d**). Values represent the mean ± s.e.m. $^{*}P<0.05$; $^{**}P<0.01$ (Tukey test). Experiments were replicated at least two times.

results suggest that mepenzolate could achieve its ameliorative effect by suppressing PPE-induced inflammatory responses.

We then focused on NF-κB and its regulator, HDAC2. The level of the Ser536-phosphorylated (active) form of NF-κB detected by immunohistochemical analysis increased in response to the PPE treatment, and could be suppressed by the simultaneous treatment of animals with mepenzolate (Fig. 5c). The level of IκB-α was decreased by the PPE treatment and remained stable when mepenzolate was concomitantly administered (Fig. 5d,e).

As shown in Fig. 5f, *Hdac2* mRNA expression was suppressed by the PPE treatment and could be partially restored by the simultaneous treatment of animals with mepenzolate. This alteration was also observed at the protein level (Fig. 5d,e). Furthermore, the enzymatic activity of HDAC was also decreased by the PPE treatment and could be partially restored by the simultaneous administration of mepenzolate (Fig. 5g). These results suggest that mepenzolate achieves its anti-inflammatory activity by increasing or decreasing the activity of HDAC2 or NF-κB, respectively.

Effect of mepenzolate on superoxide anion production. Electron spin resonance (ESR) analysis was employed to examine the effect of mepenzolate on the production of superoxide anions in mice. As shown in Fig. 6a,b, the peak amplitude corresponding to the superoxide anion level was higher in cells prepared from PPE-administered mice than in those from control mice. The peak amplitude in cells prepared from mice administered both PPE and mepenzolate was lower than that of mice administered PPE only (Fig. 6a,b), suggesting that mepenzolate suppresses the PPE-induced production of superoxide anions in the lung. The NADPH oxidase activity of cells in BALF was increased by the PPE treatment and could be partially suppressed by the simultaneous treatment of animals with mepenzolate (Fig. 6c). This suppression was observed at 4, 8 and 24 h but not 1 h after the administration of mepenzolate (Fig. 6c), suggesting that mepenzolate is a modulator of NADPH activation, but not an enzyme inhibitor of NADPH oxidase. On the other hand, the mRNA and protein expression of SOD1 and the enzymatic activity of SOD in the lung were decreased by the PPE treatment, with these effects also suppressed by the simultaneous

© 2013 Macmillan Publishers Limited. All rights reserved.

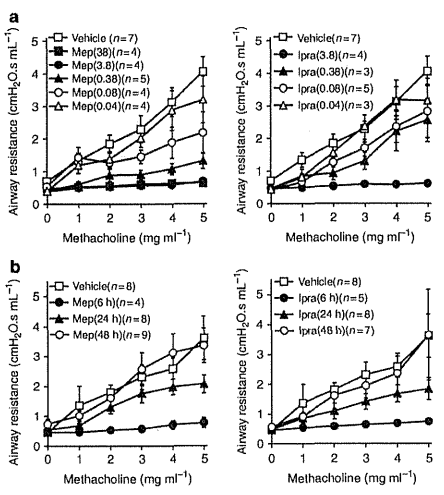

Figure 4 | Effect of mepenzolate on methacholine-induced airway constriction. Indicated doses (μg kg^{-1}) (**a**) or 38 μg kg^{-1} (**b**) of mepenzolate (Mep) or ipratropium (Ipra) were administered intratracheally. After 1 h (**a**) or indicated period (**b**), mice were exposed to nebulized methacholine five times and airway resistance was determined after each methacholine challenge as described in the Materials and Methods. Values are mean ± s.e.m. Experiments were replicated at least two times.

administration of mepenzolate (Fig. 5d–g). These results suggest that mepenzolate suppresses the PPE-induced increase in superoxide anion production by modulating the activation of NADPH oxidase or activating SOD1.

We subsequently tested whether mepenzolate directly affects superoxide anion production *in vitro*. Cells prepared from the BALF of PPE-treated mice were incubated with a spin trap agent in the presence or absence of mepenzolate. As shown in Fig. 6d,e, mepenzolate decreased the level of superoxide anions in a dose-dependent manner, the extent of which was similar to that seen with apocynin (an inhibitor of NADPH oxidase). We found that the intratracheal administration of apocynin partially suppressed PPE-induced airspace enlargement and alterations of lung mechanics (Supplementary Fig. S3). These findings suggest that most of the superoxide anions were produced by NADPH oxidase under these conditions and that mepenzolate could modulate NADPH oxidase activity and thus reduce the production of superoxide anions and PPE-induced pulmonary disorders.

To understand the mechanism of the inhibitory effect of mepenzolate on NADPH oxidase activity, we examined the effect of mepenzolate on the PPE-dependent alteration of mRNA expression of genes related to NADPH oxidase (such as *p91^{phox}(Nox2)*, *p22^{phox}*, *p40^{phox}*, *p47^{phox}*, *p67^{phox}* and *Rac2*). As shown in Supplementary Fig. S4a, PPE treatment upregulated the mRNA expression of these genes in a manner that could be suppressed by concomitant administration of mepenzolate. The mRNA expression of some of other *Noxs* (*Nox1, 4*) and dual oxidases (*Duoxs*; *Duox1, 2*) was also affected by treatment with PPE and/or mepenzolate (Supplementary Fig. S4b). Furthermore, treatment of cells in BALF with phorbol 12-myristate 13-acetate (PMA) activated NADPH oxidase, whereas pretreatment of cells with mepenzolate decreased this activity in the presence of PMA treatment but not in its absence (Fig. 6f). This finding supports the notion that mepenzolate is a modulator of NADPH activation, but not an enzyme inhibitor of NADPH oxidase. Taken together, these results suggest that the modulatory effect of mepenzolate on NADPH oxidase activity can be explained in terms of its downmodulation of the expression of NADPH oxidase-related genes and the activation of this enzyme.

To further understand the mechanism governing the mepenzolate-dependent decrease in inflammatory responses and oxidative stress, we performed DNA microarray analysis of lung tissue from mepenzolate-treated (or control) mice. Among the genes whose expression was altered by the mepenzolate administration (Table 1), we focused on genes encoding GSTs that were included in a 'glutathione metabolism' gene set (Supplementary Fig. S5a,b) and are known to reduce oxidative stress by decreasing lipid peroxide levels[9]. As shown in Fig. 7a,b, the mRNA expression of *Gst* genes and GST activity in the lung were increased by the mepenzolate administration. The mepenzolate administration also restored GST activity, which was decreased by the PPE treatment (Fig. 7c). It was reported that GST and its regulatory transcription factor, NF-E2-related factor 2 (Nrf2), in macrophages have an important role in the pathogenesis of COPD[25,26]. Therefore, we performed the Gene Set Enrichment Analysis using the custom gene set and confirmed that the downstream genes of Nrf2 (NFE2L2 target genes) were upregulated by the mepenzolate administration (Supplementary Fig. S5c,d). Furthermore, we found that treatment of RAW264 cells (a macrophage cell line) with mepenzolate upregulated the mRNA expression *Gst* genes and GST activity (Fig. 7d,e). Mepenzolate also activated Nrf2 and the expression of other Nrf2-regulated genes (heme oxygenase 1 (*Ho1*), NAD(P)H dehydrogenase, quinone1 (*Nqo1*) and *Sod1*) in RAW264 cells (Fig. 7f,g). These results suggest that the stimulatory effect of mepenzolate on Nrf2 activity and the resulting expression of *Gst* genes also involve the mepenzolate-dependent decrease in inflammatory responses and oxidative stress.

Effect of mepenzolate on CS-induced pulmonary disorders. Finally, we examined the effect of the intratracheal administration of mepenzolate on CS-induced pulmonary disorders. As shown in Fig. 8a–c, pulmonary inflammatory responses and airspace enlargement were induced following exposure of mice to CS, with the simultaneous intratracheal administration of mepenzolate clearly suppressing the severity of these CS-induced pulmonary disorders. We also found that the exposure of mice to CS decreased total respiratory system elastance and tissue elastance and that these parameters could be clearly improved by the simultaneous administration of mepenzolate (Fig. 8d). Administration of mepenzolate also suppressed CS-induced increases in oxidative stress (the pulmonary level of 8-hydroxy-2′-deoxyguanosine (8-OHdG)) (Fig. 8e). Mepenzolate increased GST activity in either the presence or absence of CS treatment *in vivo* (Fig. 8f). *In vitro*, GST activity was increased by the treatment of cells with mepenzolate, even in the presence of CS extract (CSE), which itself activated GST (Fig. 8g). On the other hand, we found that mepenzolate suppressed the CS-induced mRNA expression of *Mip-2* and *Kc* and activation of NADPH oxidase (Supplementary Fig. S6a,b). Mepenzolate also restored the HDAC and SOD activities that were decreased by exposure to CS (Supplementary Fig. S6c). These results suggest that mepenzolate protects against CS-induced pulmonary disorders *via* a mechanism similar to that in which it exerts its action against PPE-induced pulmonary disorders.

© 2013 Macmillan Publishers Limited. All rights reserved.

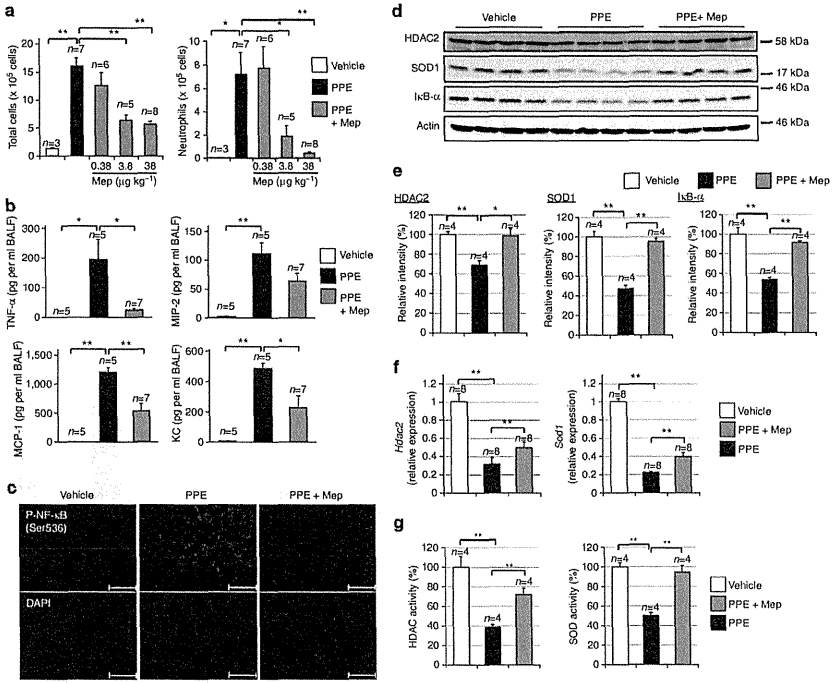

Figure 5 | Effect of mepenzolate on PPE-induced inflammatory responses. Indicated doses (μg kg^{-1}) of mepenzolate (Mep) were administered intratracheally once only. Mice were treated with or without (vehicle) PPE (100 μg per mouse) 1 h after the mepenzolate administration. Twenty-four hours after the PPE administration, BALF (**a**,**b**), sections (**c**) or homogenates (**d**–**g**) were prepared from the lung. The total cell number and the number of neutrophils (**a**) or levels of cytokines and chemokines (**b**) were determined as described in the Materials and Methods. Immunohistochemical analysis with an antibody against the Ser536-phosphorylated form of NF-κB was performed as described in the Materials and Methods (scale bar, 100 μm) (**c**). Samples were analysed by immunoblotting with antibodies against HDAC2, SOD1, IκB-α or actin (**d**). The band intensity of each protein was determined and normalized with respect to actin (**e**). Total RNA was extracted and subjected to real-time RT-PCR using a specific primer set for each gene. Values were normalized to the *Gapdh* gene and expressed relative to the control sample (**f**). The activity of HDAC or SOD was determined as described in the Materials and Methods (**g**). Values represent the mean ± s.e.m. $^{*}P<0.05$; $^{**}P<0.01$ (Tukey test). Experiments were replicated at least two times.

Discussion

The number of drugs reaching the marketplace each year is decreasing, mainly because of the unexpected adverse effects of potential drugs being revealed at advanced stages of clinical trials. To circumvent this, we have proposed a new strategy for drug discovery and development, which focuses on the use of medicines that have already been approved for use by humans (drug repositioning)[27]. In this strategy, compounds with clinically beneficial pharmacological activity are screened from a library of medicines already in clinical use to be developed for new indications. The advantage of this strategy is that there is a decreased risk for unexpected adverse effects in humans because the safety aspects of these drugs have already been well characterized in humans[27]. In the present study, we applied this strategy to screen for drugs to combat COPD. The drug mepenzolate was identified using this approach, and we found that its intratracheal administration suppresses PPE-induced airspace enlargement and alteration of lung mechanics, suggesting that mepenzolate could provide an effective treatment for COPD.

To highlight the potential clinical relevance of our findings, we performed several key experiments. First, we demonstrated that inhalation of mepenzolate was also effective against PPE-induced airspace enlargement and alteration of lung mechanics. This route of administration is noteworthy because of its potential to have less impact on the quality of life of COPD patients given that the drug can be administered on a daily basis at home. Second, we showed that mepenzolate has a therapeutic effect even when the drug was administered after the development of emphysema. We also showed that mepenzolate suppresses the PPE-induced decrease in $FEV_{0.05}$/FVC and finally, we demonstrated that mepenzolate exerts an ameliorative effect against CS-induced pulmonary disorders.

Among the five types of muscarinic receptors ($M_{1-5}R$), M_3R expressed in bronchial smooth muscle can be blocked by

© 2013 Macmillan Publishers Limited. All rights reserved.

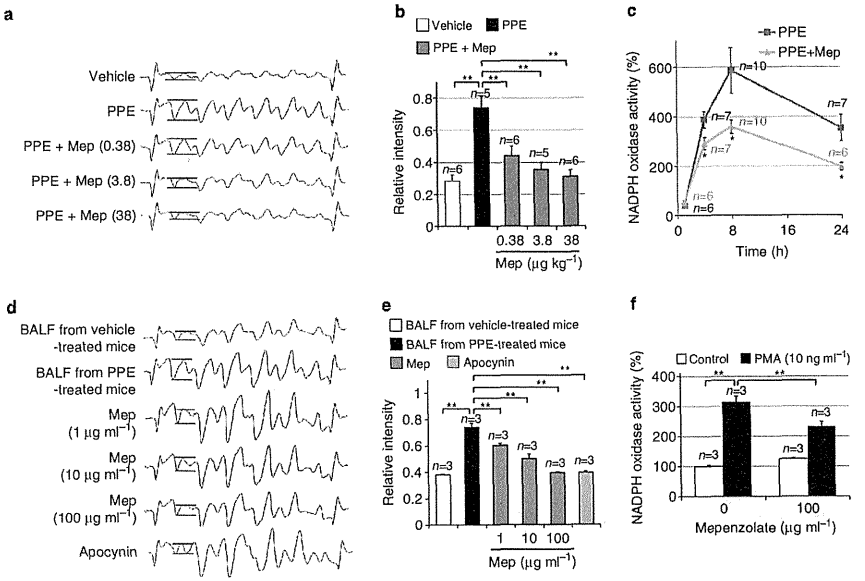

Figure 6 | Effect of mepenzolate on superoxide anion production. (**a**–**c**), indicated doses (μg kg^{-1}) of mepenzolate (Mep) were administered intratracheally once only. Mice were treated with or without (vehicle) PPE (100 μg per mouse) 1 h after the mepenzolate administration. Cells in BALF were prepared 24 h (**a**,**b**) or 1, 4, 8, 24 h (**c**) after the PPE administration. Cells were incubated with a spin trap agent (DPhPMPO) for 10 min and subjected to radical adduct ESR spectrum analysis to determine the amount of superoxide anions present. The intensity of the ESR signal of the superoxide anion adduct (DPhPMPO-OOH adduct shown by the separation between the bars in the spectra shown in (**a**)) was determined (**b**). NADPH oxidase activities in cells were determined as described in the Materials and Methods and expressed relative to vehicle-treated controls (**c**). (**d**–**f**), mice were treated once only with or without (vehicle) PPE (100 μg per mouse) and cells in BALF were collected 24 h later. Cells were incubated with DPhPMPO in the presence of indicated concentrations of mepenzolate (μg ml^{-1}) or 100 μM apocynin for 60 min. The level of superoxide anions was determined as described above (**d**,**e**). Cells were pre-incubated with or without mepenzolate (100 μg ml^{-1}) for 3 h and further incubated with NADPH in the presence or absence of PMA (10 ng ml^{-1}) for 20 min. NADPH oxidase activity was determined as described above (**f**). Values represent the mean ± s.e.m. $^{*}P<0.05$; $^{**}P<0.01$ (Tukey test). Experiments were replicated at least two times.

Table 1 | List of gene sets that were differently expressed at 25 h after administration of mepenzolate.

Gene set	NES*,†	P-value†	FDR‡
Ribosome	2.866	<0.001	<0.001
T-cell receptor signaling pathway	2.066	<0.001	0.018
Drug metabolism cytochrome P450	2.030	<0.001	0.015
Metabolism of xenobiotics by cytochrome P450	1.947	<0.001	0.023
Proteasome	1.799	0.007	0.073
Protein export	1.750	0.021	0.085
Oxidative phosphorylation	1.635	<0.001	0.160
Fatty acid metabolism	1.627	0.023	0.149
Glutathione metabolism	1.567	0.028	0.195
Parkinson's disease	1.471	0.013	0.239

*NES, normalized enrichment score.
†P-value, a permutation test implemented in Gene Set Enrichment Analysis (GSEA).
‡FDR, false discovery rate.

muscarinic antagonists, resulting in bronchodilation[28]. Thus, it is reasonable to speculate that mepenzolate, a subtype-non-specific muscarinic receptor antagonist, has bronchodilatory activity as confirmed here. Other subtype-non-specific muscarinic receptor antagonists such as ipratropium and tiotropium examined here did not exert ameliorative effects against PPE-induced pulmonary disorders. Furthermore, scopolamine (a subtype-non-specific muscarinic receptor antagonist) and pirenzepine (an M_1R-specific antagonist) also had no discernible effects against PPE-induced pulmonary disorders, even though, as for mepenzolate, these drugs are orally administered drugs used to treat gastrointestinal disorders and their clinical doses (100 mg per day per adult) are similar to that of mepenzolate (45 mg per day per adult). We also found that the M_2R-specific antagonist gallamine triethiodide and the M_3R-specific antagonist 1,1-dimethyl-4-diphenylacetoxypiperidinium iodide did not affect the PPE-induced increase in number of total leukocytes or neutrophils in BALF (Supplementary Fig. S7). These results suggest that mepenzolate achieves its ameliorative effect against PPE-induced pulmonary disorders *via* mechanisms that are independent of its muscarinic receptor and bronchodilatory activities. On the other hand, glycopyrronium suppressed PPE-induced airspace enlargement and alterations of lung mechanics. The chemical structure of glycopyrronium is similar

© 2013 Macmillan Publishers Limited. All rights reserved.

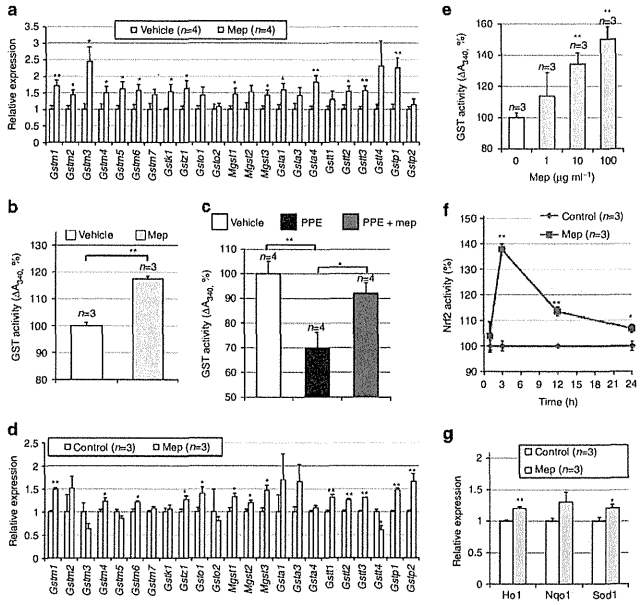

Figure 7 | Effect of mepenzolate on *Gst* gene expression and GST activity. (**a**–**c**), mepenzolate (Mep) (38 μg kg^{-1}) or vehicle (PBS) was administered intratracheally once only. Mice were treated with or without PPE (100 μg per mouse) 1 h after the mepenzolate administration (**c**). Twenty-five hours after the mepenzolate administration, lung homogenates was prepared. Total RNA was extracted and subjected to real-time RT-PCR using a specific primer set for each gene. Values were normalized to the *Hprt* gene and expressed relative to the control sample (**a**). The GST activity was determined as described in the Materials and Methods and expressed relative to the control sample (**b**,**c**). (**d**–**g**), RAW264 cells were incubated for 24 h (**d**,**e**,**g**) or indicated period (**f**) with or without (control) 100 μg ml^{-1} (**d**,**f**,**g**) or indicated doses (**e**) of mepenzolate (Mep). The mRNA expression of each gene was monitored as described above (**d**,**g**). Activities of GST and Nrf2 were determined as described in the Materials and Methods and expressed relative to the control sample (**e**,**f**). Values represent the mean ± s.e.m. $^{*}P<0.05$; $^{**}P<0.01$ (Student's *t*-test (**a**,**b**,**d**–**g**), Tukey test (**c**)). Experiments were replicated at least two times.

to that of mepenzolate (Supplementary Fig. S8), suggesting that this common structure may underlie their anti-inflammatory activities.

Mepenzolate suppressed both PPE- and CS-induced inflammatory responses. We found that the pulmonary level of the active forms of NF-κB or IκB-α increased or decreased, respectively, in response to the treatment of mice with PPE, and that the simultaneous treatment of animals with mepenzolate partially suppressed these alterations. We also found that HDAC2 and HDAC activities were decreased by the PPE treatment of mice and that simultaneous treatment with mepenzolate partially suppressed these decreases. This finding suggests that NF-κB and HDAC2 have important roles in the inhibitory effect of mepenzolate on inflammatory responses.

We also observed that treatment of mice with mepenzolate suppressed the PPE- induced increases in oxidative stress, NADPH oxidase activity and expression of NADPH oxidase-related genes. The incubation of cultured cells retrieved from BALF exhibited decreased superoxide anion production and PMA-induced activation of NADPH oxidase when the incubation was carried out in the presence of mepenzolate. However, mepenzolate did not affect the background level of NADPH oxidase activity. These results suggest that mepenzolate suppresses the PPE-induced production of superoxide anions *via* the modulation of NADPH oxidase activation and expression of NADPH oxidase-related genes. It was reported that polymorphisms in genes encoding GSTs affect the pathogenesis of COPD,[29] and we here found that mepenzolate increased the expression of *Gst* genes and GST activity in the lung. We also found that treatment of RAW264 cells with mepenzolate increased the expression of *Gst* genes and GST and Nrf2 activities. These results suggest that the mepenzolate-dependent decrease in the pulmonary level of oxidative stress *in vivo* also involves its stimulatory effect on Nrf2 and the resulting expression of *Gst* genes. It should be noted that both the modulatory effect of mepenzolate on NADPH oxidase activation and its stimulatory effect on the expression of *Gst* genes and GST activity seems not to be a secondary effect of alternative mechanisms, because these effects can be reproduced *in vitro*. Furthermore, the expression of SOD1 in the lung, which is regulated by Nrf2 (ref. 26), was decreased by the PPE treatment, and subsequently restored by the concomitant treatment of animals with mepenzolate.

This action of mepenzolate may also be involved in the observed decreased oxidative stress *in vivo*. Oxidative stress activates

© 2013 Macmillan Publishers Limited. All rights reserved.

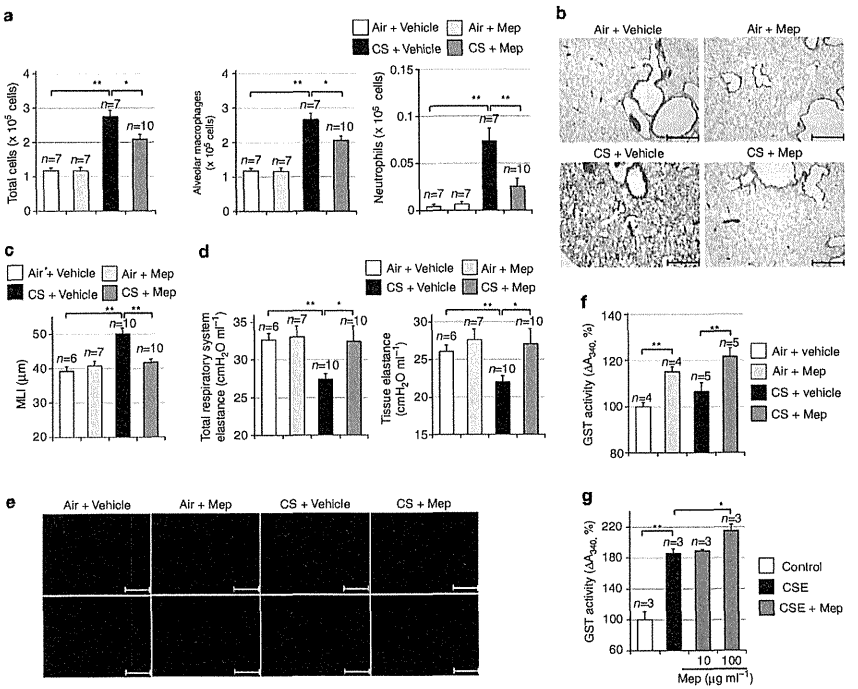

Figure 8 | Effect of mepenzolate on CS-induced pulmonary disorders. (**a**–**f**), mice were exposed to CS (three times per day) and intratracheally administered mepenzolate (Mep; 38 μg kg^{-1}, once daily) for 3 days (**a**, **f**) or for 6 months (5 days per week (from Monday to Friday)) (**b**–**e**) as described in the Materials and Methods. Only CS exposure was performed in the last week (**b**–**e**). The total cell number and the number of neutrophils or macrophages were determined as described in the Materials and Methods (**a**). Sections of pulmonary tissue were subjected to histopathological examination (H&E staining) (scale bar, 500 μm) (**b**). Airspace size was estimated by determining the MLI as described in the Materials and Methods (**c**). Total respiratory system elastance and tissue elastance were determined as described in the Methods (**d**). Immunohistochemical analysis with an antibody against 8-OHdG was performed as described in the Materials and Methods (scale bar, 200 μm) (**e**). The GST activity was determined as described in the Materials and Methods (**f**). (**g**) RAW264 cells were pre-incubated for 24 h with indicated concentrations of mepenzolate (Mep) and further incubated with CSE (15%) for 24 h. GST activity was determined as described above. Values represent the mean ± s.e.m. $^{*}P<0.05$; $^{**}P<0.01$ (Tukey test). Experiments were replicated at least two times (except for **b**–**e**).

NF-κB *via* both the inhibition of HDAC2 and the stimulation of IκB-α degradation, with these mechanisms suggested to be important for inflammatory responses associated with COPD[12,14]. Therefore, we conclude that mepenzolate suppresses inflammatory responses in animal models of COPD due to its inhibitory effect on ROS production, its stimulatory effect on the expression of antioxidant proteins and the resulting inhibition of NF-κB, which is caused by the activation of HDAC2 and the inhibition of IκB-α degradation.

As described above, a combination of anti-inflammatory drugs (such as steroids) and bronchodilators is the standard treatment regime for COPD[30,31]. We have shown that mepenzolate has both anti-inflammatory and bronchodilatory activities, suggesting that this drug could be effective for the treatment of COPD without the concomitant use of other drugs. However, the results of this study suggest that mepenzolate belongs to the short-acting muscarinic antagonists, which are used as supplemental drugs for the temporary improvement of airflow limitation[24]. On the other hand, we recently reported that steroids do not provide protective or therapeutic benefits against PPE-induced pulmonary emphysema, alterations in lung mechanics or respiratory dysfunction[23], whereas here we have shown that mepenzolate is effective against these disorders under the same experimental conditions. Based on these observations, we consider that a combination treatment regime involving the administration of long-acting muscarinic antagonists or β_2-agonists along with inhaled mepenzolate may prove to be therapeutically beneficial for COPD patients.

Methods

Chemicals and animals. Mepenzolate, PPE, PMA, glycopyrronium, ipratropium, scopolamine, N, N′-dimethyl-9, 9′-biacridinium dinitrate (lucigenin), NADPH and

© 2013 Macmillan Publishers Limited. All rights reserved.

acetyl-β-methylcholine bromide (methacholine) were obtained from Sigma (St Louis, MO). Antibodies against HDAC2, IκB-α, the Ser536-phosphorylated form of NF-κB and actin, along with apocynin were from Santa Cruz Biotechnology (Santa Cruz, CA). GeneChip Mouse Gene 1.0 ST Array was from Affymetrix (Santa Clara, CA). Alexa Fluor 594 goat anti-rabbit (or anti-mouse) immunoglobulin G was purchased from Invitrogen (Carlsbad, CA). Antibody against SOD1, gallamine triethiodide and 1,1-dimethyl-4-diphenylacetoxypiperidinium iodide and the HDAC assay kit were from Enzo Life Sciences (Farmingdale, NY). An antibody against 8-OHdG was from Nikken SEIL (Shizuoka, Japan). The GST assay kit was from PromoCell GmbH (Heidelberg, Germany). TransAM Nrf2 kit was from Active Motif (Carlsbad, CA). The SOD assay kit and the nuclear extraction hypotonic buffer were from Cayman Chemical (Ann Arbor, MI). Mounting medium for immunohistochemical analysis (VECTASHIELD) was from Vector Laboratories (Burlingame, CA). Novo-Heparin for injection was from Mochida Pharmaceutical (Tokyo, Japan). Chloral hydrate was from Nacalai Tesque (Kyoto, Japan). Diff-Quik was from the Sysmex Corporation (Kobe, Japan). ELISA kits for tumour necrosis factor-α, macrophage inflammatory protein-2, monocyte chemoattractant protein-1 and keratinocyte-derived chemokine were from R&D Systems (Minneapolis, MN). The RNeasy kit was obtained from Qiagen (Valencia, CA), the PrimeScript 1st strand cDNA Synthesis Kit was from TAKARA Bio (Ohtsu, Japan), and the SsoFast EvaGreen Supermix was from Bio-Rad (Hercules, CA). Pirenzepine dihydrochloride (pirenzepine) and formalin neutral buffer solution were from WAKO Pure Chemicals (Tokyo, Japan). Mayer's hematoxylin, 1% eosin alcohol solution and malinol were from MUTO Pure Chemicals (Tokyo, Japan). DAPI, diethylenetriamine-*N*, *N*, *N′*, *N″*, *N″*-pentaacetic acid and DPhPMPO were from Dojindo (Kumamoto, Japan). RAW264 cells (a macrophage cell line) were from RIKEN BioResource Center (Tsukuba, Japan). ICR mice (4–6 weeks old, male) and DBA/2 mice (5 weeks old, female) were purchased from Charles River (Yokohama, Japan) and used in all experiments in this paper. The experiments and procedures described here were carried out in accordance with the Guide for the Care and Use of Laboratory Animals as adopted and promulgated by the National Institutes of Health, and were approved by the Animal Care Committee of Keio University and Kumamoto University.

Preparation of BALF and CSE and cell culture. BALF was collected by cannulating the trachea and lavaging the lung with 1 ml of sterile PBS containing 50 units ml^{-1} heparin (two times). About 1.8 ml of BALF was routinely recovered from each animal. The total cell number was counted using a hemocytometer. Cells were stained with Diff-Quik reagents after centrifugation with Cytospin4 (Thermo Electron Corporation, Waltham, MA), and the ratio of neutrophils to total cell number was determined.

Cells from BALF or RAW264 cells were cultured in Eagle's minimal essential medium supplemented with 10% FBS or Eagle's minimal essential medium supplemented with 10% FBS and 0.1 mM non-essential amino acid (Lonza, Allendale, NJ), respectively, in a humidified atmosphere of 95% air with 5% CO_2 at 37 °C.

One cigarette (Peace; Japan Tobacco, Tokyo, Japan) was puffed 15 times over a 5 min period to obtain the smoke, which was bubbled into 5 ml of the culture medium using a 50-ml plastic syringe. The resulting suspension was defined 100% CSE[25].

Analyses of cytokines and chemokines and enzyme activities. Cytokine and chemokine levels were measured by ELISA according to the manufacturer's protocol. The activities of HDAC, SOD, GST and Nrf2 were measured by employing each assay kit according to the manufacturer's protocol. For the measurement of Nrf2 activity, nuclear extract was prepared as described in the manufacturer's protocol.

Measurement of level of superoxide anions. The level of superoxide anions was determined by ESR spin trapping with DPhPMPO[32,33]. Cells collected from BALF were incubated with 0.9% NaCl containing 500 μM diethylenetriamine-*N*, *N*, *N′*, *N″*-pentaacetic acid and 10 mM DPhPMPO for 10 min at 37 °C. ESR spectra were recorded at room temperature on a JES-TE200 ESR spectrometer (JEOL, Tokyo, Japan) under the following conditions: modulation frequency, 100 kHz; microwave frequency, 9.43 GHz; microwave power, 40 mW; scanning field, 330.2–340.2 mT; sweep time, 2 min; field modulation width, 0.25 mT; receiver gain, 400; and time count, 0.3 s. Every buffer and solution used in the reaction mixture used for ESR measurement was treated with Chelex 100 resin (Bio-Rad, Hercules, CA) before use to remove metal cations.

The ESR spectrum was consistent with a previously reported DPhPMPO-OOH spectrum (a hyperfine coupling constant of $a^N = 1.24$ mT, $a^H_\beta = 1.16$ mT, $a^P = 3.95$ mT)[34].

Measurement of NADPH oxidase activity. Cells in BALF were prepared as described above. NADPH oxidase activity in the cells was measured by using lucigenin as a substrate (chemiluminescence)[35]. Samples were incubated with 0.1 mM NADPH in 50 mM phosphate buffer containing 1 mM EGTA, 150 mM sucrose and 0.5 mM lucigenin, and lucigenin chemiluminescence was recorded for 15 min in a microplate reader (MicroLumat Plus LB96V, Berthold Technologies, Bad Wildbad, Germany or Infinite M1000, TECAN Group, Mannedorf, Switzerland).

Histological and immunohistochemical analyses. Lung tissue samples were fixed in 10% formalin neutral buffer solution for 24 h at a pressure of 25 cmH_2O, and then embedded in paraffin before being cut into 4 μm-thick sections.

For histological examination, sections were stained first with Mayer's hematoxylin and then with 1% eosin alcohol solution (H&E staining). Samples were mounted with malinol and inspected with the aid of an Olympus BX51 microscope (Tokyo, Japan).

To determine the MLI (an indicator of airspace enlargement), 20 lines (500 μm) were drawn randomly on the image of section stained with H&E and the intersection points with the alveolar walls were counted to determine the MLI. The morphometric analysis at the light microscopic level was conducted by an investigator blinded to the study protocol.

For immunohistochemical analysis, sections were treated with 20 μg ml^{-1} protease K for antigen activation. Sections were blocked with 2.5% goat serum for 10 min, incubated for 12 h with an antibody against the Ser536-phosphorylated form of NF-κB (1:100 dilution) or 8-OHdG (1:100 dilution) in the presence of 2.5% bovine serum albumin, and then incubated for 2 h with Alexa Fluor 594 goat anti-rabbit (or anti-mouse) immunoglobulin G (1:500 dilution) and DAPI (5 μg ml^{-1}). Samples were mounted with VECTASHIELD and inspected with the aid of a fluorescence microscope (Olympus BX51).

Immunoblotting analysis. Lung homogenates were prepared by homogenization in the buffer (50 mM Tris-HCl pH7.6, 150 mM NaCl, 1% NP-40, 1% sodium deoxycholate and 0.1% SDS) and the protein concentration of the samples was determined by the Bradford reagent[36]. Samples were applied to polyacrylamide SDS gels, subjected to electrophoresis and the resultant proteins immunoblotted with their respective antibodies. Full gel scans were shown in Supplementary Fig. S9.

Real-time RT-PCR analysis. Total RNA was extracted from lung tissues using an RNeasy kit according to the manufacturer's protocol. Samples (2.5 μg RNA) were reverse transcribed using a first-strand cDNA synthesis kit. Synthesized cDNA was used in real-time RT–PCR (Chromo 4 instrument (Bio-Rad, Hercules, CA) experiments using SsoFast EvaGreen Supermix, and analysed with Opticon Monitor Software. Specificity was confirmed by electrophoretic analysis of the reaction products and by inclusion of template- or reverse transcriptase-free controls. To normalize the amount of total RNA present in each reaction, glyceraldehyde-3-phosphate dehydrogenase or hypoxanthine guanine phosphoribosyltransferase cDNA was used as an internal standard.

Primers were designed using the Primer3 or Primer-BLAST website. The primers sequence was shown in Supplementary Table S2.

Treatment of mice with PPE and CS. ICR mice maintained under anaesthesia with chloral hydrate (500 mg kg^{-1}) were given one intratracheal injection of PPE (100 μg per mouse or 15 U kg^{-1}) in PBS *via* micropipette.

DBA/2 or ICR mice were exposed to CS by placing 10–20 mice in a chamber (volume, 45 l) connected to a CS-producing apparatus. Commercial non-filtered cigarettes (Peace; Japan Tobacco, Tokyo, Japan) that yielded 28 mg tar and 2.3 mg nicotine on a standard smoking regimen were used. Mice were exposed to the smoke of 1 cigarette for 35 min, 3 times per day, 5 days per week (from Monday to Friday) for 6 months, or to the smoke of 2 cigarettes for 25 min, 3 times per day for 3 days. The apparatus was configured such that each cigarette was puffed 15 times over a 5-min period.

For the administration of mepenzolate by inhalation, 5–8 mice were placed in a chamber (volume, 45 l) and an ultrasonic nebulizer (NE-U07, Omron, Tokyo, Japan) connected to the chamber was used to nebulize over a 30-min period the entire volume of a solution containing mepenzolate dissolved in 10 ml PBS. For control mice, PBS alone was nebulized. Mice were kept in the chamber for a further 10 min after completion of the nebulization.

For the intratracheal administration of candidate drugs, mice were maintained under anaesthesia with chloral hydrate (500 mg kg^{-1}) and each drug in PBS was administered *via* micropipette. For control mice, PBS alone was administered by the same procedure.

Unless otherwise noted, the first administration of each drug was performed 1 h prior to the PPE administration or 2 h before the CS treatment.

Analyses of lung mechanics and respiratory functions. Measurement of lung mechanics and airway resistance was performed with a computer-controlled small-animal ventilator (FlexiVent, SCIREQ, Montreal, Canada)[32,33]. Mice were anesthetized with chloral hydrate (500 mg kg^{-1}), a tracheotomy was performed, and an 8-mm section of metallic tube was inserted into the trachea. Mice were mechanically ventilated at a rate of 150 breaths per min, using a tidal volume of 8.7 ml kg^{-1} and a positive end-expiratory pressure of 2–3 cmH_2O.

Total respiratory system elastance and tissue elastance were measured by the snap shot and forced oscillation techniques, respectively. All data were analysed using FlexiVent software (version 5.3; SCIREQ, Montreal, Canada).

For measurement of the methacholine-induced increase in airway resistance, mice were exposed to nebulized methacholine (1 mg ml^{-1}) five times for 20 s with a 40-s interval between each and airway resistance was measured after each

© 2013 Macmillan Publishers Limited. All rights reserved.

methacholine challenge by the snap shot technique. All data were analysed using the FlexiVent software.

Determination of the FEV0.05/FVC ratio was performed with the same computer-controlled small-animal ventilator connected to a negative pressure reservoir (SCIREQ, Montreal, Canada)[32,33]. Mice were tracheotomized and ventilated as described above. The lungs were inflated to a pressure of 30 $cm H_2O$ over 1 s and held at this pressure. After 0.2 s, the pinch valve (connected to ventilator) was closed and after 0.3 s, the shutter valve (connected to negative pressure reservoir) was opened for exposure of the lung to the negative pressure. The negative pressure was held for 1.5 s to ensure complete expiration. FEV0.05/FVC was determined using the FlexiVent software.

Gene expression analysis using DNA microarray. Using 100 ng of total RNA extracted from lung tissues, hybridization and signal detection of GeneChip Mouse Gene 1.0 ST Arrays (Affymetrix, Santa Clara, CA) were performed following the manufacturer's instructions. Gene expression analysis was performed in duplicate for each experimental condition. The raw data were normalized by the robust multi-array average method[37] using the 'affy' package from BioConductor (http://www.bioconductor.org/) and R statistical software version 2.12.1 (http://www.r-project.org/).

For functional analysis, we used Gene Set Enrichment Analysis version 2.0.13 with MSigDB gene sets version 4.0 (ref. 38). A gene set category c2.cp.kegg based on the KEGG pathway database was used, and a custom gene set (SINGH_NFE2L2_TARGETS from the category c2.cgp) was used for the analysis of Nrf2-related gene sets. We used 'Diff_of_Classes' (the difference of class means to calculate fold change) as a metric for ranking genes. All other parameters were set to the default values, except for 'set_min' (the minimum size of gene set) to 10 for the Nrf2-related gene sets. Gene sets satisfying $P<0.05$ and FDR <0.25 were considered significant.

Statistical analysis. All values are expressed as the mean ± s.e.m. Two-way analysis of variance followed by the Tukey test or the Student's *t*-test for unpaired results was used to evaluate differences between three or more groups or between two groups, respectively. Differences were considered to be significant for values of $P<0.05$.

References

1. Rabe, K. F. *et al.* Global strategy for the diagnosis, management, and prevention of chronic obstructive pulmonary disease: GOLD executive summary. *Am. J. Respir. Crit. Care. Med.* **176,** 532–555 (2007).
2. Barnes, P. J. & Stockley, R. A. COPD: current therapeutic interventions and future approaches. *Eur. Respir. J.* **25,** 1084–1106 (2005).
3. Owen, C. A. Proteinases and oxidants as targets in the treatment of chronic obstructive pulmonary disease. *Proc. Am. Thorac. Soc.* **2,** 373–385 discussion 394-375 (2005).
4. Tashkin, D. P. *et al.* A 4-year trial of tiotropium in chronic obstructive pulmonary disease. *N. Engl. J. Med.* **359,** 1543–1554 (2008).
5. Calverley, P. M. *et al.* Salmeterol and fluticasone propionate and survival in chronic obstructive pulmonary disease. *N. Engl. J. Med.* **356,** 775–789 (2007).
6. Alsaeedi, A., Sin, D. D. & McAlister, F. A. The effects of inhaled corticosteroids in chronic obstructive pulmonary disease: a systematic review of randomized placebo-controlled trials. *Am. J. Med.* **113,** 59–65 (2002).
7. Barnes, P. J., Ito, K. & Adcock, I. M. Corticosteroid resistance in chronic obstructive pulmonary disease: inactivation of histone deacetylase. *Lancet* **363,** 731–733 (2004).
8. Drummond, G. R., Selemidis, S., Griendling, K. K. & Sobey, C. G. Combating oxidative stress in vascular disease: NADPH oxidases as therapeutic targets. *Nat. Rev. Drug. Discov.* **10,** 453–471 (2011).
9. Gosker, H. R. *et al.* Altered antioxidant status in peripheral skeletal muscle of patients with COPD. *Respir. Med.* **99,** 118–125 (2005).
10. Rahman, I. & MacNee, W. Antioxidant pharmacological therapies for COPD. *Curr. Opin. Pharmacol.* **12,** 256–265 (2012).
11. Barnes, P. J. Role of HDAC2 in the pathophysiology of COPD. *Annu. Rev. Physiol.* **71,** 451–464 (2009).
12. Rajendrasozhan, S., Yang, S. R., Edirisinghe, I., Yao, H., Adenuga, D. & Rahman, I. Deacetylases and NF-kappaB in redox regulation of cigarette smoke-induced lung inflammation: epigenetics in pathogenesis of COPD. *Antioxid. Redox. Signal.* **10,** 799–811 (2008).
13. Rahman, I. & Adcock, I. M. Oxidative stress and redox regulation of lung inflammation in COPD. *Eur. Respir. J.* **28,** 219–242 (2006).
14. Yao, H. *et al.* Redox regulation of lung inflammation: role of NADPH oxidase and NF-kappaB signalling. *Biochem. Soc. Trans.* **35,** 1151–1155 (2007).
15. Yang, S. R. *et al.* Cigarette smoke induces proinflammatory cytokine release by activation of NF-kappaB and posttranslational modifications of histone deacetylase in macrophages. *Am. J. Physiol. Lung. Cell Mol. Physiol.* **291,** L46–L57 (2006).
16. Wu, C. Chromatin remodeling and the control of gene expression. *J. Biol. Chem.* **272,** 28171–28174 (1997).
17. Ito, K. *et al.* Decreased histone deacetylase activity in chronic obstructive pulmonary disease. *N. Engl. J. Med.* **352,** 1967–1976 (2005).
18. Di Stefano, A. *et al.* Increased expression of nuclear factor-kappaB in bronchial biopsies from smokers and patients with COPD. *Eur. Respir. J.* **20,** 556–563 (2002).
19. Ito, K. *et al.* Histone deacetylase 2-mediated deacetylation of the glucocorticoid receptor enables NF-kappaB suppression. *J. Exp. Med.* **203,** 7–13 (2006).
20. Chen, J. Y. Antispasmodic activity of JB-340 (N-methyl-3-piperidyl-diphenylglycolate methobromide) with special reference to its relative selective action on the sphincter of Oddi, colon and urinary bladder of the dog. *Arch. Int. Pharmacodyn. Ther.* **121,** 78–84 (1959).
21. Buckley, J. P., De, F. J. & Reif, E. C. The comparative antispasmodic activity of N-methyl-3-piperidyl diphenylglycolate methobromide (JB-340) and atropine sulfate. *J. Am. Pharm. Assoc. Am. Pharm. Assoc. (Baltim.)* **46,** 592–594 (1957).
22. Long, J. P. & Keasling, H. H. The comparative anticholinergic activity of a series of derivatives of 3-hydroxy piperidine. *J. Am. Pharm. Assoc. Am. Pharm. Assoc. (Baltim.)* **43,** 616–619 (1954).
23. Tanaka, K. I., Sato, K., Aoshiba, K., Azuma, A. & Mizushima, T. Superiority of PC-SOD to other anti-COPD drugs for elastase-induced emphysema and alteration in lung mechanics and respiratory function in mice. *Am. J. Physiol. Lung. Cell Mol. Physiol.* **302,** L1250–L1261 (2012).
24. Hanania, N. A. & Donohue, J. F. Pharmacologic interventions in chronic obstructive pulmonary disease: bronchodilators. *Proc. Am. Thorac. Soc.* **4,** 526–534 (2007).
25. Suzuki, M. *et al.* Down-regulated NF-E2-related factor 2 in pulmonary macrophages of aged smokers and patients with chronic obstructive pulmonary disease. *Am. J. Respir. Cell Mol. Biol.* **39,** 673–682 (2008).
26. Kundu, J. K. & Surh, Y. J. Nrf2-Keap1 signaling as a potential target for chemoprevention of inflammation-associated carcinogenesis. *Pharm. Res.* **27,** 999–1013 (2010).
27. Mizushima, T. Drug discovery and development focusing on existing medicines: drug re-profiling strategy. *J. Biochem.* **149,** 499–505 (2011).
28. Belmonte, K. E. Cholinergic pathways in the lungs and anticholinergic therapy for chronic obstructive pulmonary disease. *Proc. Am. Thorac. Soc.* **2,** 297–304 discussion 311-292 (2005).
29. Xue, H., Su, J., Sun, K., Xie, W. & Wang, H. Glutathione S-transferase M1 and T1 gene polymorphism and COPD risk in smokers: an updated analysis. *Mol. Biol. Rep.* **39,** 5033–5042 (2012).
30. Gross, N. J., Giembycz, M. A. & Rennard, S. I. Treatment of chronic obstructive pulmonary disease with roflumilast, a new phosphodiesterase 4 inhibitor. *COPD* **7,** 141–153 (2010).
31. Miravitlles, M. & Anzueto, A. Insights into interventions in managing COPD patients: lessons from the TORCH and UPLIFT studies. *Int. J. Chron. Obstruct. Pulmon. Dis.* **4,** 185–201 (2009).
32. Tanaka, K., Sato, K., Aoshiba, K., Azuma, A. & Mizushima, T. Superiority of PC-SOD to other anti-COPD drugs for elastase-induced emphysema and alteration in lung mechanics and respiratory function in mice. *Am. J. Physiol. Lung. Cell Mol. Physiol.* **302,** L1250–L1261 (2012).
33. Tanaka, K. *et al.* Therapeutic effect of lecithinized superoxide dismutase on pulmonary emphysema. *J. Pharmacol. Exp. Ther.* **338,** 810–818 (2011).
34. Karakawa, T. *et al.* Applicability of new spin trap agent, 2-diphenylphosphinoyl-2-methyl-3,4-dihydro-2H-pyrrole N-oxide, in biological system. *Biochem. Biophys. Res. Commun.* **370,** 93–97 (2008).
35. Griendling, K. K., Minieri, C. A., Ollerenshaw, J. D. & Alexander, R. W. Angiotensin II stimulates NADH and NADPH oxidase activity in cultured vascular smooth muscle cells. *Circ. Res.* **74,** 1141–1148 (1994).
36. Bradford, M. M. A rapid and sensitive method for the quantitation of microgram quantities of protein utilizing the principle of protein-dye binding. *Anal. Biochem.* **72,** 248–254 (1976).
37. Irizarry, R. *et al.* Exploration, normalization, and summaries of high density oligonucleotide array probe level data. *Biostatistics.* **4,** 249–264 (2003).
38. Subramanian, A. *et al.* Gene set enrichment analysis: a knowledge-based approach for interpreting genome-wide expression profiles. *Proc. Natl Acad. Sci. USA* **102,** 15545–15550 (2005).

Acknowledgements

We thank Dr. Tomoko Betsuyaku (Keio University) for critical reading of this manuscript and Mrs. Kumi Matsuura, Mrs. Arisa Oyama and Mr. Yuri Miyazaki (Kumamoto University) for technical assistance. This work was supported by Grants-in-Aid for Scientific Research from the Ministry of Health, Labour, and Welfare of Japan, as well as the Japan Science and Technology Agency and Grants-in-Aid for Scientific Research from the Ministry of Education, Culture, Sports, Science and Technology, Japan.

Author contributions

Conception and design: K.-I.T., T.M.; analysis and interpretation: K.-I.T., T.I., T.S., D.K., Y.Y., K.I., K.M., K.S.; drafting the manuscript for important intellectual content: K.-I.T., T.I., N.Y., K.-I.T., K.M., H.T., K.S., H.S., T.M.

© 2013 Macmillan Publishers Limited. All rights reserved.

Additional information

Supplementary Information accompanies this paper at http://www.nature.com/naturecommunications

Competing financial interests: The authors declare no competing financial interests.

Reprints and permission information is available online at http://npg.nature.com/reprintsandpermissions/

How to cite this article: Tanaka, K.-I. *et al.* Mepenzolate bromide displays beneficial effects in a mouse model of chronic obstructive pulmonary disease. *Nat. Commun.* 4:2686 doi: 10.1038/ncomms3686 (2013).

© 2013 Macmillan Publishers Limited. All rights reserved.

BIOINFORMATION
Discovery at the interface of physical and biological sciences

open access www.bioinformation.net *Hypothesis*

Volume 9(8)

PathAct: a novel method for pathway analysis using gene expression profiles

Kaoru Mogushi & Hiroshi Tanaka*

Department of Bioinformatics, Division of Medical Genomics, Medical Research Institute, Tokyo Medical and Dental University 24F M&D Tower Bldg., 1-5-45 Yushima, Bunkyo-ku, Tokyo, Japan; Hiroshi Tanaka – Email: tanaka@bioinfo.tmd.ac.jp; Phone: +81-3-5803-5839; *Corresponding author

Received April 14, 2013; Accepted April 16, 2013; Published April 30, 2013

Abstract:
We developed PathAct, a novel method for pathway analysis to investigate the biological and clinical implications of the gene expression profiles. The advantage of PathAct in comparison with the conventional pathway analysis methods is that it can estimate pathway activity levels for individual patient quantitatively in the form of a pathway-by-sample matrix. This matrix can be used for further analysis such as hierarchical clustering and other analysis methods. To evaluate the feasibility of PathAct, comparison with frequently used gene-enrichment analysis methods was conducted using two public microarray datasets. The dataset #1 was that of breast cancer patients, and we investigated pathways associated with triple-negative breast cancer by PathAct, compared with those obtained by gene set enrichment analysis (GSEA). The dataset #2 was another breast cancer dataset with disease-free survival (DFS) of each patient. Contribution by each pathway to prognosis was investigated by our method as well as the Database for Annotation, Visualization and Integrated Discovery (DAVID) analysis. In the dataset #1, four out of the six pathways that satisfied $p < 0.05$ and FDR < 0.30 by GSEA were also included in those obtained by the PathAct method. For the dataset #2, two pathways ("Cell Cycle" and "DNA replication") out of four pathways by PathAct were commonly identified by DAVID analysis. Thus, we confirmed a good degree of agreement among PathAct and conventional methods. Moreover, several applications of further statistical analyses such as hierarchical cluster analysis by pathway activity, correlation analysis and survival analysis between pathways were conducted.

Background:
Gene expression profiling by microarray analysis provides a huge amount of biological information and has been widely used in biological and clinical research. Since microarray technique simultaneously detects expression levels for more than ten thousand of genes, bioinformatics approaches for interpretation of such large-scale data are essential. The microarray data is often examined using the information of a pathway, which represents a series of biological reactions that causes a specific event such as signal transduction, cell proliferation, and drug metabolism. There are several pathway databases such as the KEGG PATHWAY database **[1]**, BioCarta **[2]** and GenMAPP **[3]**. In addition, Gene Ontology (GO) database **[4]** provides controlled vocabularies of various genes and has a hierarchical structure based on their functions. Recently, several interpretation tools such as gene set enrichment analysis (GSEA) **[5]**, the Database for Annotation, Visualization and Integrated Discovery (DAVID) **[6]**, GenMAPP **[3]**, and GOMiner **[7]** have been developed and widely used in the microarray analysis. The majority of tools for pathway analysis detect pathway-level difference between two groups (e.g., cases and controls). The output results generated by these tools are typically given as a list of p-values and other software-specific information, which is not suitable for further analyses. If the activity (i.e., the degree of up- and down-regulation) of a pathway can be estimated in each samples, these information would be of great use for investigation of patient-specific characteristics of a disease and further development of personalized medicine. In this study, a novel method for pathway analysis, called PathAct, is introduced. PathAct can estimate individual pathway activity by conversion of gene expression data into quantitative values for both of each pathway and each sample. One of the most unique features is that the output data is given in matrix form, which can be used for further analysis such as hierarchical clustering and other multivariate analysis methods.

© 2013 Biomedical Informatics

The median polish (MP) algorithm **[8]**, which is a core component in PathAct, is a suitable method for an additive decomposition of a two-dimensional data matrix. MP is known as an exploratory data analysis for extraction of both row-wide and column-wide trends from a two-dimensional matrix. MP is an iterative procedure that consists of the following four steps: (1) calculating median values of each row, (2) subtracting the median values from each row, (3) calculating median values of each column, and (4) subtracting the median values from each column. These steps are repeated using the residual matrix as a new data, and the median vectors for the row and the column are accumulated at each iteration. This procedure is iterated until the reduction of the sum of absolute residual is less than a specified value, or the maximum limit of iteration is exceeded. The MP method has been used for several bioinformatics tools including the robust multi-array average (RMA) method **[9]**, one of the most well-known normalization methods for DNA microarray data.

Methodology:
PathAct algorithm
Application of the MP method to microarray data is formularized as follows. Suppose that a pathway p contains N_p genes, and M samples are obtained from the microarray experiment. Note that a gene may belong to multiple pathways. For the $N_p \times M$ gene expression matrix G_p, the expression intensity of the i-th gene for the j-th individual is denoted as $G_p[i, j]$. Using MP, G_p is decomposed into a gene effect $g_p[i]$, an individual effect $a_p[j]$, and an residual matrix $R_p[i, j]$, $G_p[i, j] = g_p[i] + a_p[j] + R_p[i, j]$; The individual effect a_p is the pathway activity and is used for further analysis. The gene effect g_p reflects a degree of bias such as hybridization efficiency of each gene. When a database contains K pathways, these steps are repeated for K times to produce the $K \times M$ pathway activity matrix A by collecting a_p of each pathway. These procedures, namely PathAct, were implemented in R statistical language version 2.15.2 (http://www.r-project.org/). The program is freely available upon request. A dataset including 229 human pathways was obtained from the KEGG PATHWAY database using an R packages "KEGG.db" and "hgu133plus2.db". "KEGG.db" contains information about KEGG PATHWAY entry such as pathway IDs and names, whereas "hgu133plus2.db" is an annotation data for Affymetrix HG-133 plus 2.0 array including pathway information. When multiple probe sets correspond to a single gene, a probe set with the largest interquartile range (IQR) was selected as a responsible probe set for the gene. Termination conditions of each MP process were set to 1% as a change of absolute residual and ten times as the maximum iteration steps.

Application to clinical microarray datasets
To evaluate the feasibility of our pathway analysis method, two public microarray datasets were downloaded from the Gene Expression Omnibus (GEO) database (http:// www.ncbi.nlm.nih.gov/geo/). The dataset #1 (GSE19615) contains a total of 115 gene expression profiles obtained from tissue specimens of breast cancer patients **[10]** using HG-133 Plus 2.0 arrays. The data have clinicopathological information for estrogen receptor (ER), progesterone receptor (PR), and human epidermal growth factor receptor 2 (HER2) expressions. Triple-negative breast cancer (TNBC), which does not express ER, PR, and HER2, is associated with higher risk of distant metastasis and poor prognosis compared to other type of breast cancer (non-triple-negative breast cancer; NTNBC) **[11]**. Therefore, we aimed to identify pathways differently activated between TNBC and NTNBC. The gene expression profiles including 54,613 probe sets were converted into a pathway activity matrix using PathAct. Association between pathway activities and TNBC was determined by the Wilcoxon exact rank-sum test provided by "exactRankTests" package in R. Then, pathways with at least 1.1-fold increase or decrease between TNBC and NTNBC were further selected. The dataset #2 (GSE21653) contains a total of 266 gene expression profiles from breast cancer patients using HG-133 Plus 2.0 arrays **[12]**. Among them, 252 patients had information for disease-free survival (DFS), which was calculated from the date of diagnosis until date of first relapse or date of death (when the relapse was not observed). These gene expression profiles were also converted into a pathway activity matrix using PathAct, and we investigated pathways associated with DFS using Cox proportional hazards model. In both datasets, pathways satisfying both $p < 0.05$ by Wald test and FDR < 0.30 were considered statistically significant.

Comparison with conventional pathway analysis methods
For the dataset #1, we investigated pathways associated with TNBC by gene set enrichment analysis (GSEA) **[5]**. We used a collection of gene sets for KEGG pathways provided by MSigDB 3.1 (c2.cp.kegg.v3.1.symbols.gmt, available at http://www.broadinstitute.org/gsea/msigdb/). Pathways that satisfied both $p < 0.05$ and FDR < 0.30 were selected and were compared with the results obtained by PathAct. In the second analysis using dataset #2, as GSEA cannot conduct survival analysis, we first extracted genes related to DFS by Cox proportional hazards model using a cut-off value of $p < 0.05$ by Wald test. Then, the selected genes were analyzed by DAVID Functional Annotation Tool **[6]** version 6.7. We used the "KEGG_PATHWAY" category provided by DAVID for analysis of pathways that were overrepresented by the genes associated with DFS. Two separate analyses were performed for the genes up-regulated in poor prognosis patients (hazards ratio (HR) > 1 by the Cox regression) and for those down-regulated in poor prognosis patients (HR < 1). Pathways that satisfied both $p < 0.05$ and FDR < 0.30 by DAVID analysis were then selected.

Discussion:
Pathway-based analysis of TNBC dataset
Using the dataset #1, we calculated the pathway activity matrix of 229 KEGG pathways for the 115 patients by the PathAct method. We then identified 15 up-regulated and 13 down-regulated pathways in TNBC by comparing the pathway activity values between TNBC and NTNBC. Using the calculated pathway activity levels, we next performed a hierarchical cluster analysis using the above 28 pathways **(Figure 1A)**. When the patients were classified into two major clusters, the left cluster contained four TNBC and 61 NTNBC patients, whereas the right cluster contained 26 TNBC and 24 NTNBC patients ($p < 0.001$ by Fisher's exact test). This indicates that the PathAct method can summarize the important molecular information in breast cancer, a part of which is necessary for classification of TNBC from NTNBC.

© 2013 Biomedical Informatics

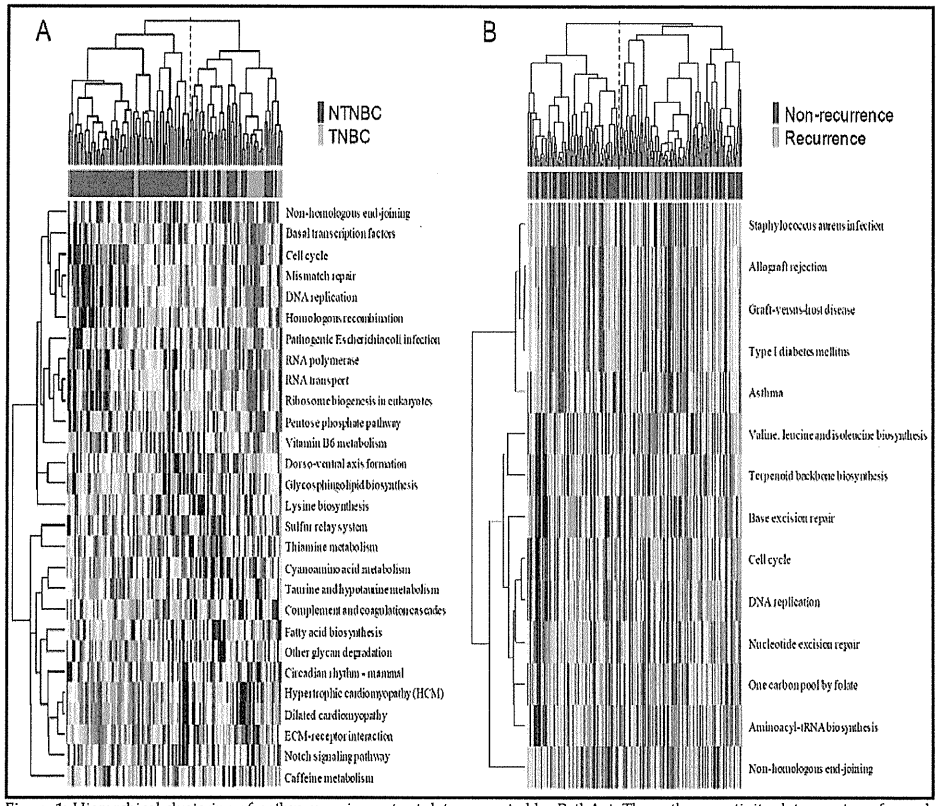

Figure 1: Hierarchical clustering of pathways using output data generated by PathAct. The pathway activity data was transformed into z-scores by setting the mean expression intensities to 0 and variances to 1 for all pathways. The Euclidean distance was used to calculate a similarity matrix among pathways or individuals, respectively. The red dashed lines indicate the two major clusters obtained by the hierarchical cluster analysis. A: a hierarchical cluster analysis using the selected 28 pathways for the dataset #1. B: a hierarchical cluster analysis using the selected 14 pathways for the dataset #2.

Pathways associated with TNBC

The pathways associated with cell proliferation (e.g., "DNA replication" and "Cell cycle") and transcription process (e.g., "Basal transcription factors" and "RNA polymerase") were significantly up-regulated in TNBC **Table 1 (see supplementary material).** This suggests that the cancer cells in TNBC are more aggressive than those in other type of cancer. On the other hand, the pathway "ECM-receptor interaction", related to cell adhesion, was down-regulated in TNBC **Table 1.** Because loss of cell adhesion promotes migration, invasion and metastasis of cancer cells, the down-regulation of these pathways suggested the higher metastatic ability of TNBC than NTNBC. It has been reported that TNBC are further classified into several subtypes such as basal-like, normal-like, and claudin-low subtypes **[13]**. Among them, the claudin-low subtype shows lower mRNA expression levels of cell cycle-related genes **[14].** As shown in **Figure 1A**, a part of TNBC patient's exhibits lower activity levels of cell cycle-related Pathways, which suggest the existence of subtypes among TNBC patients.

Pathway-based analysis of DFS in breast cancer

Using the dataset #2, we also obtained the pathway activity matrix of 229 KEGG pathways for the 266 patients by the PathAct method. Using the pathway activity levels, we selected 14 pathways that had significant association with DFS **Table 2 (see Supplementary material).** Among these pathways, nine showed hazard ratio (HR) > 1, and the other five had HR < 1. Similar to the analysis of the dataset #1, we conducted a

© 2013 Biomedical Informatics

hierarchical cluster analysis using the selected 14 pathways **(Figure 1B).** When the patients were divided into the two clusters, the left cluster contained 27 recurrence and 80 recurrence-free patients, whereas the right cluster contained 56 recurrence and 89 recurrence-free patients (p = 0.030 by Fisher's exact test). This indicated that the patients in the right cluster had significantly higher risk of tumor recurrence.

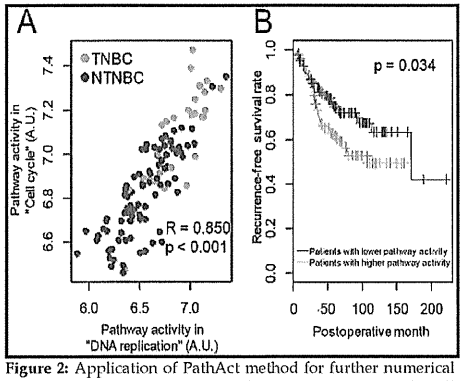

Figure 2: Application of PathAct method for further numerical analysis. A: correlation analysis of "DNA replication" and "Cell cycle" for the dataset #1 (p < 0.001 by Pearson's correlation test). B: analysis of correlation between DFS and the pathway activity in "Allograft rejection". Down-regulation of this pathway contribute to better prognosis (p = 0.034 by log-rank test).

Pathways associated with prognosis of breast cancer

The pathways associated with cell proliferation (e.g., "DNA replication", "Base excision repair", and "Cell cycle") were positively correlated with poor prognosis **Table 2.** Promotion of cell proliferation in cancer is a typical phenomenon in carcinogenesis and cancer progression. On the other hand, the five pathways for better prognosis contained "Asthma" and "Graft-versus-host disease", which did not seem to be associated with cancer. However, these pathways include genes related to immune response process such as antigen processing (e.g., MHC class II genes) and cytokines (e.g., IL2, 4, 5, and 9). This suggested that the immune response function in cancerous tissue was activated in patients with better prognosis compared with patients with poor prognosis. In fact, it has been reported that breast cancer patients with a higher number of tumor-infiltrating CD8(+) lymphocytes shows better prognosis **[15].** Therefore, activation of these pathways in patients with good prognosis is possibly caused by increased number of lymphocytes by lymphocytic infiltration.

Comparison to conventional methods

In order to validate the PathAct method, we compared the analysis results of the datasets #1 and #2 with other approaches. First, we performed GSEA for the dataset #1 and identified six pathways that were significantly altered in TNBC **Table 3 (see supplementary material).** Interestingly, four out of six pathways identified by GSEA were also included in those obtained by the PathAct method. Therefore, we confirmed that GSEA and PathAct had ability to detect common biological pathways in the microarray dataset. Next, we evaluated pathways associated with DFS in the dataset #2. Using Cox proportional hazards model, 1,487 probe sets were identified to be negatively correlated with DFS, whereas 1,081 probe sets had positive correlation with DFS. DAVID analysis was then performed for each of the selected gene sets **Table 4 (see supplementary material.** "Cell Cycle" and "DNA replication" pathways were significantly overrepresented in genes associated with poor prognosis, and these were also detected by the PathAct method. Similarly, 13 pathways were identified for genes correlated with good prognosis, and four pathways associated with immune response ("Asthma", "Graft-versus-host disease", "Allograft rejection", and "Type I diabetes mellitus") were also detected by the PathAct. Thus, we confirmed good agreement between PathAct and DAVID.

Quantitative analyses using pathway activities

A major advantage of PathAct method is that obtained pathway activity levels can be used for further statistical analysis. For example, the correlation analysis of "DNA replication" and "Cell cycle" for the dataset #1 was performed **(Figure 2A).** These two pathways showed significant correlation (p < 0.001 by Pearson's correlation test), and both pathways were up-regulated in TNBC compared with NTNBC. Another example is an analysis of correlation between DFS and the pathway activity in "Allograft rejection" **(Figure 2B).** When the median value of the pathway activity levels was chosen for a cut-off point, it was demonstrated that up-regulation of this pathway contribute to better prognosis (p = 0.034 by log-rank test). Because the "Allograft rejection" pathway contains many genes associated with immune response, this result infers that increased number of lymphocytes by lymphocytic infiltration could contribute to the better prognosis of the breast cancer patients.

Conclusion:

Pathway analysis plays an important role in interpreting genome-wide gene expression data. Several methods for pathway analysis have been proposed, but they are restricted to making comparisons between groups. Thus, the development of a flexible evaluation framework for individual patients is crucial for the advanced interpretation of microarray data. In this study, a novel approach for estimating individual pathway activity using the median polish algorithm was introduced. Using the clinical microarray datasets, the capability of the PathAct method was evaluated. The PathAct method could detect the similar pathways with those obtained by the conventional methods such as GSEA and DAVID. Moreover, because the processed data (i.e., the pathway activity matrix) are given as quantitative values for both of each pathway and each sample, they could be utilized for further statistical analysis including analysis of correlation and survival data. Therefore, PathAct is a promising tool for pathway-level investigation and interpretation of the comprehensive gene expression data.

Conflict of interest:

No conflict of interest was declared.

Acknowledgement:

The authors would like to thank Dr. Ken Miyaguchi for a critical reading of this manuscript.

© 2013 Biomedical Informatics

Reference:
[1] Kanehisa M & Goto S, *Nucleic Acids Res.* 2000 **28:** 27 [PMID: 10592173]
[2] Nishimura D, *Biotech Softw Internet Rep.* 2001 **2:** 117
[3] Dahlquist KD *et al. Nat Genet.* 2002 **31:** 19 [PMID: 11984561]
[4] Ashburner M *et al. Nat Genet.* 2000 **25:** 25 [PMID: 10802651]
[5] Subramanian A *et al. Proc Natl Acad Sci USA.* 2005 **102:** 15545 [PMID: 16199517]
[6] Huang da W *et al. Nat Protoc.* 2009 **4:** 44 [PMID: 19131956]
[7] Zeeberg BR *et al. Genome Biol.* 2003 **4:** R28 [PMID: 12702209]
[8] Malo N *et al. Nat Biotechnol.* 2006 **24:** 167 [PMID: 16465162]
[9] Irizarry RA *et al. Biostatistics.* 2003 **4:** 249 [PMID: 12925520]
[10] Li Y *et al. Nat Med.* 2010 **16:** 214 [PMID: 20098429]
[11] Dent R *et al. Clin Cancer Res.* 2007 **13:** 4429 [PMID:17671126]
[12] Sabatier R *et al. Breast Cancer Res Treat.* 2011 **126:** 407 [PMID: 20490655]
[13] Lehmann BD *et al. J Clin Invest.* 2011 **121:** 2750 [PMID: 21633166]
[14] Prat A *et al. Breast Cancer Res.* 2010 **12:** R68 [PMID: 20813035]
[15] Mahmoud SM *et al. J Clin Oncol.* 2011 **29:** 1949 [PMID: 21483002]

Edited by P Kangueane
Citation: Mogushi & Tanaka, Bioinformation 9(8): 394-400 (2013)
License statement: This is an open-access article, which permits unrestricted use, distribution, and reproduction in any medium, for non-commercial purposes, provided the original author and source are credite

© 2013 Biomedical Informatics

BIOINFORMATION open access

Supplementary material:

Table 1: List of pathways associated with TNBC using PathAct.

Pathway	p-value	FDR	Fold
Up-regulated pathways in TNBC			
DNA replication	<0.001	<0.001	1.272
Cell cycle	<0.001	<0.001	1.202
Mismatch repair	<0.001	<0.001	1.183
Ribosome biogenesis in eukaryotes	<0.001	<0.001	1.185
Vitamin B6 metabolism	<0.001	<0.001	1.457
RNA transport	<0.001	<0.001	1.115
Basal transcription factors	<0.001	<0.001	1.118
Pathogenic Escherichia coli infection	<0.001	<0.001	1.149
Homologous recombination	<0.001	0.002	1.105
Glycosphingolipid biosynthesis - lacto and neolacto series	<0.001	0.004	1.113
Pentose phosphate pathway	0.001	0.011	1.121
RNA polymerase	0.001	0.011	1.116
Dorso-ventral axis formation	0.001	0.012	1.135
Non-homologous end-joining	0.008	0.032	1.101
Lysine biosynthesis	0.016	0.051	1.200
Down-regulated pathways in TNBC			
Hypertrophic cardiomyopathy (HCM)	<0.001	<0.001	0.905
Notch signaling pathway	<0.001	<0.001	0.877
Circadian rhythm - mammal	<0.001	<0.001	0.851
Dilated cardiomyopathy	<0.001	0.001	0.905
Fatty acid biosynthesis	<0.001	0.001	0.826
ECM-receptor interaction	<0.001	0.003	0.832
Taurine and hypotaurine metabolism	0.001	0.008	0.854
Cyanoamino acid metabolism	0.001	0.008	0.834
Other glycan degradation	0.001	0.009	0.887
Sulfur relay system	0.002	0.012	0.893
Caffeine metabolism	0.006	0.027	0.871
Thiamine metabolism	0.010	0.038	0.894
Complement and coagulation cascades	0.011	0.040	0.904

Table 2: List of pathways associated with DFS by PathAct.

Pathway	HR (95% CI)	p-value	FDR
Negative correlation with DFS			
DNA replication	2.049 (1.235-3.399)	0.005	0.217
Base excision repair	3.130 (1.366-7.168)	0.007	0.217
Non-homologous end-joining	4.533 (1.491-13.78)	0.008	0.217
Aminoacyl-tRNA biosynthesis	3.353 (1.373-8.186)	0.008	0.217
Cell cycle	2.535 (1.257-5.112)	0.009	0.217
Nucleotide excision repair	2.818 (1.288-6.164)	0.009	0.217
Valine, leucine and isoleucine biosynthesis	2.536 (1.206-5.336)	0.014	0.279
Terpenoid backbone biosynthesis	2.203 (1.169-4.153)	0.015	0.279
One carbon pool by folate	2.593 (1.196-5.624)	0.016	0.279
Positive correlation with DFS			
Asthma	0.343 (0.159-0.737)	0.006	0.217
Graft-versus-host disease	0.526 (0.327-0.847)	0.008	0.217
Staphylococcus aureus infection	0.573 (0.378-0.868)	0.009	0.217
Allograft rejection	0.545 (0.345-0.862)	0.009	0.217
Type I diabetes mellitus	0.520 (0.304-0.891)	0.017	0.284

Table 3: TNBC-associated pathways analyzed by GSEA.

Pathway	Size	NES*	p-value	FDR
Aminoacyl trna biosynthesis	32	1.928	<0.001	0.063
Cell cycle	113	1.869	<0.001	0.069

© 2013 Biomedical Informatics

RNA degradation	51	1.735	0.037	0.206
DNA replication	34	1.698	0.031	0.216
Basal transcription factors	33	1.696	0.020	0.175
Glycosphingolipid biosynthesis lacto and neolacto series	26	1.663	0.011	0.196

* NES, normalized enrichment score.

Table 4: List of pathways associated with DFS identified by DAVID.

Pathway	Size	%	p-value	FDR
Negative correlation with DFS				
hsa04110:Cell cycle	21	2.41	< 0.001	< 0.001
hsa03030:DNA replication	9	1.03	< 0.001	0.025
Positive correlation with DFS				
hsa05330:Allograft rejection	12	3.90	< 0.001	< 0.001
hsa05332:Graft-versus-host disease	12	3.90	< 0.001	< 0.001
hsa04940:Type I diabetes mellitus	12	3.90	< 0.001	< 0.001
hsa04612:Antigen processing and presentation	15	4.87	< 0.001	< 0.001
hsa05310:Asthma	10	3.25	< 0.001	< 0.001
hsa05320:Autoimmune thyroid disease	12	3.90	< 0.001	< 0.001
hsa04672:Intestinal immune network for IgA production	11	3.57	< 0.001	< 0.001
hsa05416:Viral myocarditis	12	3.90	< 0.001	< 0.001
hsa05322:Systemic lupus erythematosus	12	3.90	< 0.001	< 0.001
hsa04514:Cell adhesion molecules (CAMs)	13	4.22	< 0.001	< 0.001
hsa04640:Hematopoietic cell lineage	7	2.27	0.005	0.055
hsa00340:Histidine metabolism	4	1.30	0.017	0.149
hsa05340:Primary immunodeficiency	4	1.30	0.028	0.219

© 2013 Biomedical Informatics

A Map of Alzheimer's Disease–Signaling Pathways: A Hope for Drug Target Discovery

S Ogishima[1], S Mizuno[1], M Kikuchi[2], A Miyashita[3], R Kuwano[3], H Tanaka[1,2] and J Nakaya[1]

Alzheimer's disease (AD) is a complex neurodegenerative condition, and its drug therapy is challenging. To inform AD drug discovery, we developed the "AlzPathway," a prototype of a comprehensive map of AD-related signaling pathways, from information obtained through studies in the public domain. The AlzPathway provides an integrated platform for systems analyses of AD-signaling pathways and networks.

PATHWAY-BASED DRUG DISCOVERY AND A MAP OF DISEASE-SIGNALING PATHWAYS

Over the past decade, whole-genome sequencing and other omics technologies have revealed pathogenic gene mutations, aberrant mRNA expressions, and dysfunctional signaling pathways, which then have yielded novel targets for a new generation of drugs, e.g., "molecularly targeted drugs." This strategy has succeeded to some extent but with limitations. Many molecularly targeted drugs have been found to be ineffective in spite of favorable pharmacokinetics or to cause significant target-related side effects.[1] In renewed efforts to address these limitations, "pathway-based drug discovery" has been proposed for examinations of the complicated system behavior of pathogenic signaling affected by drugs.

A comprehensive map of pathogenic signaling pathways would be informative for pathway-based drug discovery. Comprehensive maps have already been constructed to reveal pathogenesis and to develop drugs in the fields of cancer and immunological disease; such maps include those for particular signals such as epidermal growth factor receptor, retinoblastoma (RB)/E2F, Toll-like receptor, mammalian target of rapamycin, and dendritic cell signals.

Nearly 36 million people were suffering from dementia worldwide as of 2010, and this figure is expected to increase to 65.7 million by 2030.[2] The societal costs of dementia are already huge and could continue to increase rapidly. Clearly, the development of AD drugs is an urgent need. However, despite major efforts and funding, the development of AD drugs has remained a great challenge. We therefore undertook this project of developing the first comprehensive AD signaling map to contribute to the broader goal of developing drugs to combat and prevent AD.

CONSTRUCTION OF ALZPATHWAY

We collected 123 review articles involving AD and curated them manually to construct a first comprehensive map of AD-signaling pathways (AlzPathway)[3] using the modeling software CellDesigner (http://celldesigner.org/),[4] a modeling editor for biochemical pathways. The number of articles in PubMed involving AD over the past 50 years is more than 80,000. We therefore chose review articles as information sources for practical reasons.

AlzPathway is described based on the process description of Systems Biology Graphical Notation.[3] AlzPathway is provided as both a standardized Systems Biology Markup Language map for communicating and storing computational models of biological processes, and as a high-resolution image map, available at http://alzpathway.org/. For community-driven updates of the AlzPathway map, it is also provided as a Web service map using a community-based, collaborative Web service platform called Payao (http://payao.oist.jp).[5] AD researchers can continuously correct and update AlzPathway in a collaborative manner using the Payao Web service map.

AD-SIGNALING PATHWAYS

An overview of the AlzPathway map is given in Figure 1. The AlzPathway map comprises 1,347 species, 1,070 reactions, and 129 phenotypes. The molecules are classified as follows: 650 proteins, 232 complexes, 223 simple molecules, 32 genes, 36 RNAs, 24 ions, and 21 degraded products. The reactions are classified as 401 state transitions, 22 transcriptions, 30 translations, 172 heterodimer associations, 49 dissociations, 87 transports, 20 unknown transitions, and 228 omitted transitions.[3] There are 34 canonical pathways in AlzPathway, such as amyloid precursor protein, mitochondrial, and apoptosis pathways; these contain the following AD hallmark pathways: amyloid-β cleavage, amyloid-β degradation, and

[1]Department of Bioclinical Informatics, Tohoku Medical Megabank Organization, Tohoku University, Sendai-shi, Japan; [2]Department of Bioinformatics, Tokyo Medical and Dental University, Tokyo, Japan; [3]Department of Molecular Genetics, Center for Bioresources, Brain Research Institute, Niigata University, Niigata, Japan. Correspondence: S Ogishima (ogishima@sysmedbio.org)

Received 2 January 2013; accepted 14 February 2013; advance online publication 20 March 2013. doi:10.1038/clpt.2013.37

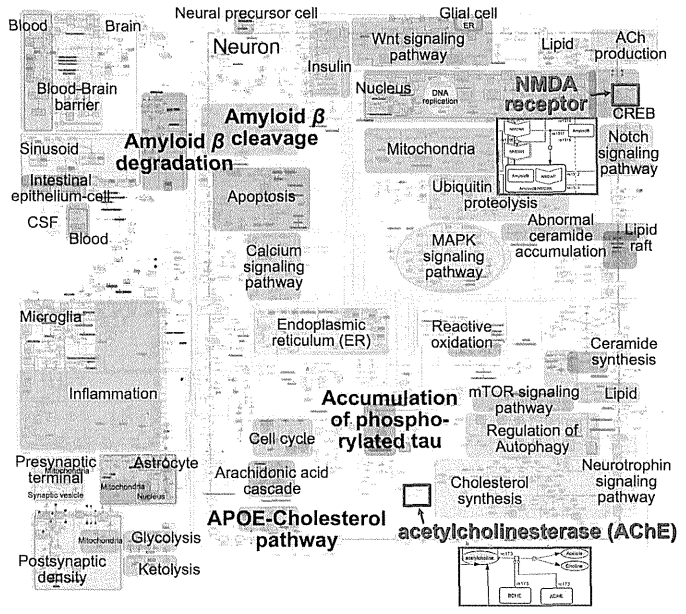

Figure 1 Overview of AlzPathway map overlaid with canonical pathway annotations and drug targets of the existing US Food and Drug Administration–approved drugs, acetylcholinesterase and the *N*-methyl-D-aspartic acid receptor. No compensation pathway and no undesired pathway have been identified around these drug targets. ACh, acetylcholine; APOE, apolipoprotein E; CREB, cAMP response element-binding; CSF, cerebrospinal fluid; MAPK, mitogen-activated protein kinases; mTOR, mammalian target of rapamycin; NMDA, *N*-methyl-D-aspartate receptor.

apolipoprotein E–cholesterol pathways, and neurofibrillary tangles accumulation.[3] AlzPathway is the first comprehensive map of signaling pathways of a particular disease that catalogs not only intra- but also inter- and extracellular signaling pathways among neurons, glial cells, microglia, presynaptic cells, postsynaptic cells, astrocytes, and the blood–brain barrier.[3]

KEY MOLECULES IN THE AD PATHWAY AS DRUG TARGETS

To find key molecules in the AD pathway, we represented the AlzPathway in binary-relation notation (Figure 2). In Systems Biology Graphical Notation, a reaction is composed of reactant(s), modifier(s), and product(s). In binary-relation notation, a reaction is decomposed into a binary relation between (i) reactant(s) and product(s), and (ii) modifier(s) and product(s).

In accord with the edge betweenness centrality of binary relations, we highlighted molecules with high centrality relations as key molecules (Figure 2). Betweenness centrality is a measure of a node centrality in a network and is defined as the number of the shortest paths from all nodes to all other nodes that go through that node. Highlighted key molecules were amyloid-β, apolipoprotein E, microtubule-associated protein-τ, and γ-secretase. The γ-secretase generates amyloid-β 1–40, leading to amyloid-β oligomers that are crucial for AD progression. These molecules are considered key molecules in the AD pathogenic pathway.

From the point of view of pathway-based drug discovery, a drug targeting a key molecule might be effective but could also cause significant side effects as a result of off-target or unintended downstream effects. In fact, the development of semagacestat, a γ-secretase inhibitor, was discontinued in phase III trials because of an increased risk of skin cancer as compared with the placebo. It was not known that γ-secretase has other targets, e.g., peripheral Notch, or that the inhibition of γ-secretase causes an increased risk of skin cancer. In AlzPathway, γ-secretase shows a relationship with Notch signaling, and it is a key molecule showing high centrality—which could cause significant downstream effects on unintended molecules and pathways, if perturbed (Figure 2). AlzPathway provides comprehensive knowledge of AD pathogenesis and signaling pathways, and informs us of a possibility of off-target effects within the network.

Tacrine, rivastigmine, galantamine, donepezil, and memanatine are the only drugs currently approved by the US Food and Drug Administration to treat the symptoms of AD. These drugs are cholinesterase inhibitors (tacrine, rivastigmine, galantamine, and donepezil) or an *N*-methyl-D-aspartic acid receptor antagonist